Sandia
National
Laboratories

SAND92-7009

WIND LOAD DESIGN METHODS FOR GROUND BASED HELIOSTATS and PARABOLIC DISH COLLECTORS

By J.A. Peterka and R.G. Derickson

Issued by Sandia National Laboratories, operated for the United States Department of Energy by Sandia Corporation.

Available to DOE and DOE contractors from
Office of Scientific and Technical Information
PO Box 62
Oak Ridge, TN 37831

Prices available from (615) 576-8401, FTS 626-8401

Available to the public from
National Technical Information Service
US Department of Commerce
5285 Port Royal Rd
Springfield, VA 22161

NTIS price codes
Printed copy: A03
Microfiche copy: A01

SAND--92-7009

DE93 002737

SAND92-7009
Unlimited Release
Printed September 1992

WIND LOAD DESIGN METHODS FOR GROUND-BASED HELIOSTATS AND PARABOLIC DISH COLLECTORS

J.A. Peterka
R.G. Derickson
Fluid Mechanics and Wind Engineering Program
Fluid Dynamics and Diffusion Laboratory
Department of Civil Engineering
Colorado State University
Fort Collins, CO 80523

Sandia Contract 69-1865

ABSTRACT

The purpose of this design method is to define wind loads on flat heliostat and parabolic dish collectors in a simplified form. Wind loads are defined for both mean and peak loads accounting for the protective influence of upwind collectors, wind protective fences, or other wind-blockage elements. The method used to define wind loads was to generalize wind load data obtained during tests on model collectors, heliostats or parabolic dishes, placed in a modeled atmospheric wind in a boundary-layer wind tunnel at Colorado State University. For both heliostats and parabolic dishes, loads are reported for solitary collectors and for collectors as elements of a field. All collectors were solid with negligible porosity; thus the effects of porosity in the collectors is not addressed.

ACKNOWLEDGEMENTS

Development of this document was supported by Sandia National Laboratories under contract 69-1865. The active support and guidance of Mr. Jim Grossman of Sandia Laboratories is acknowledged. The data contained herein were developed under other contracts with Sandia, the Solar Energy Research Institute (now the National Renewable Energy Laboratory) and other sources as referenced within the document.

TABLE OF CONTENTS

LIST OF TABLES

LIST OF FIGURES

LIST OF FIGURES (cont.)

WIND LOAD DESIGN METHODS FOR GROUND BASED HELIOSTATS AND PARABOLIC DISH COLLECTORS

J. A. Peterka[1] and R. G. Derickson[2]

INTRODUCTION

Optimum design of isolated units or fields of heliostats and parabolic dish collectors is dependent upon obtaining realistic design wind loads. In the future these structures may become even more sensitive to wind loads as gravity loads decrease through innovative technology.

The purpose of this design method is to define wind loads on flat heliostats and parabolic dish collectors in a simplified form. Wind loads are defined for both mean and peak loads accounting for the protective influence of upwind collectors, wind protective fences, or other wind blockage elements. The method used to define wind loads was to generalize wind load data obtained during tests on model collectors, heliostats or parabolic dishes, placed in a modeled atmospheric wind in a boundary-layer wind tunnel at Colorado State University. For both heliostats and parabolic dishes, loads are reported for solitary collectors and for collectors as elements of a field. All collectors were solid with negligible porosity. Thus the effects of porosity in the collectors is not addressed.

This methodology is based on experimental research performed for Sandia National Laboratories and the Solar Energy Research Institute (now the National Renewable Energy Laboratory) over a period of several years, Peterka et al.

---

[1] Professor, Fluid Mechanics and Wind Engineering Program, Colorado State University, Fort Collins, CO 80523.

[2] Graduate Student, Fluid Mechanics and Wind Engineering Program, Colorado State University.

(1990, 1988, 1987 and 1986), and earlier references cited therein. A summary of these efforts is provided in Peterka et al. (1990 and 1989). The measured mean and peak wind loads have been compiled and presented here in a simplified design procedure that should provide realistic design guidance for the range of module shapes and field layouts considered. This methodology represents current research knowledge which may be modified through future research.

The user of this design method is encouraged to become familiar with the various principles, assumptions, and limitations of application outlined herein.

Design parameters for heliostats and parabolic dish collectors are contained in separate tables or sections to minimize confusion. It is not exhaustive in its treatment of case scenarios. It is possible that higher loads than those outlined herein are possible, although wind-tunnel tests were designed to identify the higher load cases. The geometries studied were idealized and did not have attached to them all of the truss structures which might be on a production unit. It is not clear that truss structure loads are simply additive to loads shown herein. In many cases that assumption will be valid -- in others, the truss structure might significantly modify the wind flow about the collector and thus the loads as calculated in this document (including possible significant load decreases).

The design methods outlined in this document are based only on wind-tunnel tests. While wind-tunnel tests have proven highly useful in defining wind loads, it must be emphasized that full-scale validating experiments would be highly desirable, in view of the high sensitivity of loads to turbulence (gustiness in the wind) observed in the wind-tunnel tests. The procedures proposed herein are not intended to replace but to supplement existing codes, standards, and other design methods and procedures.

ATMOSPHERIC WINDS

Discussions of atmospheric wind flow and its physical model simulation can be found in Simiu and Scanlan (1986), Counihan (1975), Cermak (1971, 1975), and Reinhold (ed., 1982). A brief summary of the important characteristics for use in this document are summarized below. Some material is included for educational purposes and to clarify reasons for the design approach suggested in this document.

Several types of atmospheric winds can lead to design level winds on a solar collector. Strong low pressure areas can generate design level winds. These are called extratropical lows if their origin is in temperate regions; their winds are the normal straight line winds with which we are most familiar. Low pressures of tropical origin give rise to tropical cyclones which are indistinguishable from extra-tropical lows unless they become strong enough to be classified as tropical storms or hurricanes. Tornados are concentrated rotational winds with a relatively small spatial extent of high speed; the weaker ones could be resisted by a solar collector, but more intense versions are not within the normal design range of solar collectors. Dust devils are also rotational winds similar to a tornado, but with lower speeds, which typically originate with a clear sky as opposed to a storm origin for tornadoes. Downslope wind storms occur in local areas in the lee of some mountain ranges and can reach speeds above hurricane magnitude.

Winds of interest for solar collector design have some common characteristics near the ground. Mean (time averaged) wind speed increases with height above ground, and winds have gusts of short duration which are significantly higher than the mean and which define peak wind loads on solar collectors. Both the variation of speed with height and the gustiness, frequently called turbulence, must be accounted for in the design of solar

collectors. For example, wind load coefficients determined by wind tunnel in a flow without vertical variation of speed and without significant turbulence, such as ASCE (1961), are not appropriate for design. The quantitative impact of proper modeling will be shown in the section on atmospheric turbulence.

Design of solar collectors for wind outlined in this document assumes a boundary layer structure to the wind; the classical example is the straight line winds of the extra-tropical low or tropical cyclone. The structure of the wind for other types of high wind event is not as well known, but is assumed to be similar enough to the boundary layer structure for design purposes. Boundary layer wind tunnels capable of simulating the structure of boundary layer winds are available for modeling wind loads on structures, and have been used to define wind loads on various solar collector shapes. The results of several research test series were used in development of this design methodology.

In an atmospheric boundary layer wind, the variation of wind speed with height is frequently represented by a power law

$$U(Z)/U(Zref) = (Z/Zref)^n$$

where

$U(Z)$ = mean velocity at height Z;

$u(Zref)$ = mean velocity at reference height Zref; and

n = power law exponent, a measure of ground roughness; 0.13 to 0.15 in open country.

An alternate expression which works well is the logarithmic law

$$U(Z)/U_* = (1/k)\ \ln(Z/Z_o)\ .$$

A form of this equation for transferring mean velocities between heights is

$$U(Z)/U(Zref) = \ln(Z/Z_o)/\ln(Zref/Z_o)$$

where

U_* = the shear velocity;

k = von Kàrmàn constant, 0.4;

ln = natural log function; and

Z_o = effective roughness length, another measure of ground roughness; 0.01 to 0.05 meters in open country.

An expression for turbulence is (Simiu and Scanlan, 1986)

$$Tu = (B)(U_*)/U(Z)$$

where

B = a constant, approximately 2.5 for open country.

Examples of ground surface roughness characteristics are included as Table 1. This table is for informational purposes; it is not explicitly used in the design methodology of this document.

Gust velocities of 2 to 3 second duration can be related to mean velocities at 10 meters height in open country by

$$Upk(10m) = (R)\ U(10m)$$

where

Upk(10m) = 2-3 second gust magnitude at 10 m; and

R = constant, 1.53 to 1.6 in open country.

MEASURED PEAK AND QUASI-STEADY PEAK WIND LOADS

Wind load codes and standards have traditionally assumed a "quasi-steady" wind load in which a time averaged, or mean, load coefficient is used with a peak gust wind speed to determine peak wind loads. The "quasi-steady" approach assumes that the short duration peak wind load is essentially a "steady" wind load. If that assumption were strictly true, then we would obtain the same load by using a mean wind with a measured peak coefficient. Experiments have shown that the "quasi-steady" assumption works well for some cases, for example the

Table 1. Estimated values of the surface roughness.

z_o (m)	Representative Value of z_o (m)	Terrain	n	Turbulence Intensity, % at 10 m*
0.5-1.5	0.7	Center of large towns, cities, forests	0.35	34
		Dense forests of relatively non-uniform height	0.27-0.30**	34
		Dense forests of relatively uniform height	0.23-0.25**	34
0.15-0.5	0.3	Small towns, suburban area	0.24	26
0.05-0.15	0.1	Wooded country villages, outskirts of small towns, farmland	0.20	21
0.015-0.05	0.03	Open country with isolated trees and buildings	0.17	17
0.007-0.015	0.01	Grass, very few trees	0.15	14
0.0015-0.007	0.003	RUNWAY AREAS (Average) Surface covered with snow, rough sea in storm	0.13	13
<0.0015	0.001	Calm open sea, lakes, snow covered flat terrain. Flat desert	0.11	11

*Turbulence intensities calculated from information in Simiu et al. (1986)
z_o = effective surface roughness
n = power law exponent for mean velocity variation with elevation

**All roughness entries in table except these are from ESDU (1982)

peak force where mean force is large. The peak force is essentially the gust factor in wind, squared, times the mean force.

For other cases the "quasi-steady" assumption does not work well at all. For example, the mean moment about the elevation axis for a flat heliostat in stow position (horizontal orientation with minimum area exposed to wind) is quite low. The fluctuating part of the moment leading to the peak value oscillates about the near-zero mean and is due in large part to vertical components of the turbulent approach flow. Thus the peak moment is determined mainly by the fluctuating part of the moment and is not predicted well by a gust factor (representing the square of the ratio of actual wind gust to mean wind speed) multiplied by the mean.

For reasons given above, it is best to determine peak loads by using a measured peak coefficient in combination with the mean wind. Load coefficients are thus defined using the dynamic pressure, Q, of the mean wind speed. Since both mean and peak wind loads may be of interest, this document includes both mean and peak coefficients.

SPECIFICATION OF DESIGN WIND SPEEDS

Since wind speed varies with height above ground, with gust duration and with upwind surface ground roughness, it is important that the wind speeds used for collector design be specified for height, duration and exposure. A clear specification of required wind speed might be: X miles per hour mean hourly wind at 10 meters above ground in open country, or a peak gust of Y miles per hour at 10 meters height in open country. A peak gust typically means the highest point traced on an anemometer recording chart which is about a 2 to 3 second duration gust. For a straight line boundary layer wind, the peak gust is about 1.6 times the mean hourly wind based on Hollister (1970) and about 1.53 times the hourly

speed based on ANSI/ASCE 7-88 (1988). Conversion of mean wind from one height to another is performed using the wind profile equations listed above. Peak winds follow a different profile.

Converting winds from one exposure to another is not completely straightforward. If the upwind ground roughness is constant for 5 to 10 kilometers, then the conversion can be accomplished by

$$Ur = Uo\ (Zgo/Z10)^{no}\ (Z10/Zgr)^{nr}$$

where

Ur = mean speed at 10 meters in roughness r exposure;

Uo = mean speed at 10 meters in open country exposure;

Zgo = effective gradient height in open country exposure;

Zgr = effective gradient height in roughness r exposure;

Z10 = 10 meters, standard specification height for wind;

no = power law exponent for open country, 0.143; and

nr = power law exponent for roughness r exposure.

Consistent pairs for Zgr and nr (Zgo and no for open country) taken from ANSI/ASCE 7-88 are:

Exposure Category	Zgr,meters	nr
A - Large City Centers	450	0.333
B - Urban and Suburban Areas	350	0.222
C - Open Country	275	0.143
D - Flat Unobstructed Coastal Areas	210	0.100

It is recommended herein that collectors be designed for an open country environment and that design wind requirements be specified also at 10 meters in open country environment. The primary reason to change the exposure would be for collectors located on the edge of a large body of water or on exposed terrain (hilltops, ridges) where wind speeds might be higher than in open country.

Hilltop exposures have special problems (not addressed herein) in defining wind speeds due to accelerated flows.

PRINCIPLES OF WIND LOADING

Structural failure from wind loads can be due to different mechanisms. One type is overstressing in which the peak stresses induced by the near static wind loads exceed the material capacity. Measurement of peak loads in the studies leading to this method provide a method for design against over-stressing failure. Fatigue failure can be caused by dynamic, repeated loading at stresses less than the static, allowable material capacity. Fatigue design is not addressed in this methodology. Fatigue is not explicitly addressed in Peterka et al. (1990 and 1989), but the range of fluctuating load magnitudes for many critical situations is shown in figures in these two references. The load spectra, or frequency distribution of loads, was not measured.

Mean loads are defined as an average over a period ranging from 10 minutes to an hour. Values of these loads are reported herein. However, it is the peak fluctuating loads that provide the stresses for design. Peak forces may be a result of peak, near-static applied wind loads, or may be due to static or dynamic wind loads augmented by resonant vibrations in the structure. Resonant additions to the applied wind loads of this design method may be significant if structural damping is low. The research studies leading to this method included only determination of peak applied wind loads and did not include the prediction of resonant effects. The importance of resonant effects is not clear, since aerodynamic damping due to collector motion (resistance to motion caused by velocity of the collector through the air) may limit resonance. As the natural frequency of collector increases, any resonant response will decrease.

With respect to resonant loads, one reviewer of this document made the following comment which was sufficiently significant that it is included here verbatim: "I must highly emphasize to designers of large pedestal supported arrays that resonant vibrations must be considered. In our earlier designs, we experienced several drive failures in the field when only static wind loads were considered in the design. Naturally we were forced to consider dynamic effects to correct the problems."

COORDINATE SYSTEM OF COLLECTORS - Forces and Moments

The coordinate systems for a heliostat or parabolic dish collector are the same. Forces or moments for either an isolated or in-field collector are based on the same set of equations. In the equations, the values of the various coefficients differ, depending on a particular isolated or in-field collector configuration. Particular coefficient values for isolated or in-field heliostats and parabolic dishes are presented later.

Based on the coordinate system shown in Figure 1, the defining set of equations are as follows (forces in lb, moments in lb-ft):

Drag Force: $F_x = C_{F_x} * Q * A$ (1)

Lift Force: $F_z = C_{F_z} * Q * A$ (2)

Base Overturning Moment: $M_y = C_{M_y} * Q * A * H$ (3)

Hinge Moment: $M_{H_y} = C_{MH_y} * Q * A * h$ (4)

Azimuthal Moment: $M_z = C_{M_z} * Q * A * h$ (5)

C_{M_y} is obtained from $C_{M_y} = C_{F_x} + C_{MH_y} * (h/H)$ (6)

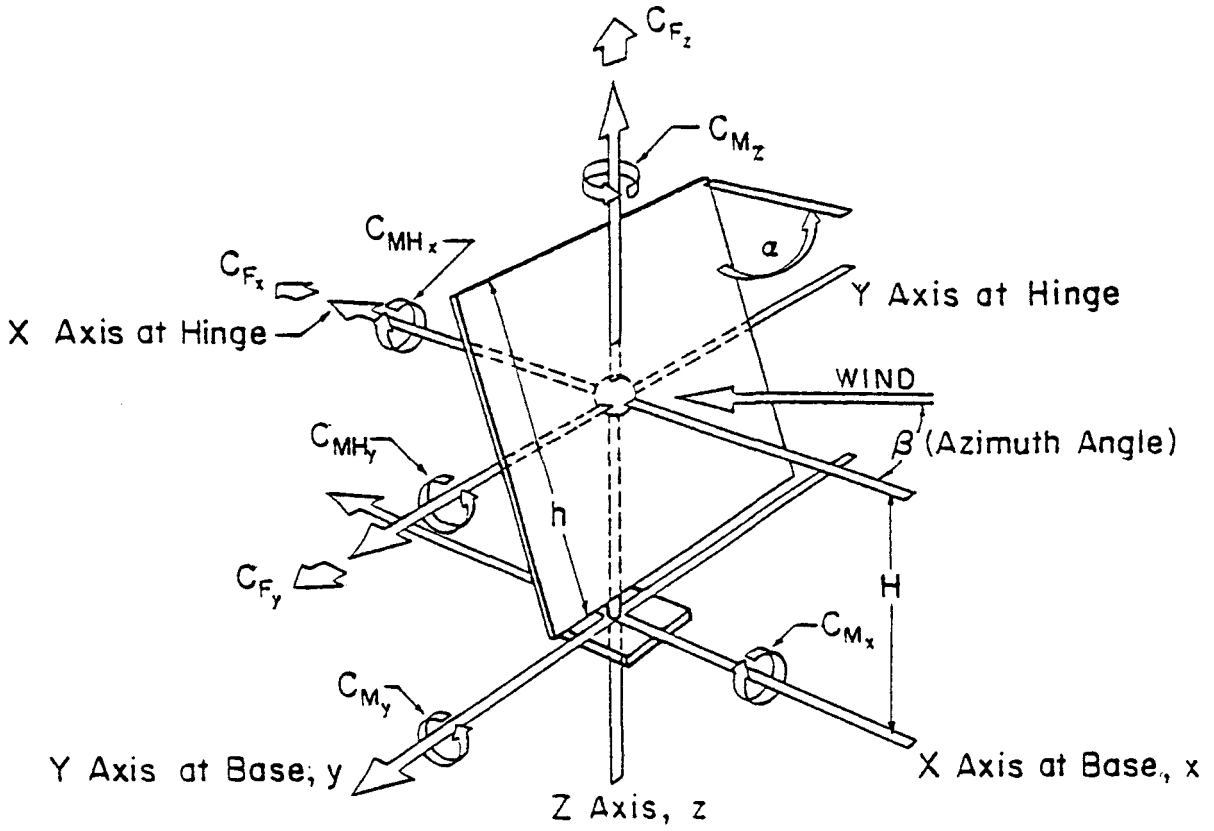

Figure 1. Coordinate system for collector (heliostat or parabolic dish).

where

Q = dynamic pressure of the mean approach wind (psf) = 0.00256 * U^2 with U in mph (0.00256 includes air density at sea level at standard conditions);

U = mean approach wind at elevation $H = U_{mean} \left[\frac{H}{Z_{wind}}\right]^n$;

n = the power law exponent for the approaching wind;

U_{mean} = mean approach wind at elevation $z_{wind} = U_{fastest\text{-}mile}/R$ or $U_{mean} = U_{gust}/1.6$;

U_{gust} = 2-3 second gust magnitude at height z_{wind} above ground;

$U_{fastest\ mile}$ = fastest mile wind speed at height z_{wind} above ground;

R = 1.30 if fastest mile wind is 90 mph
= 1.24 if fastest mile wind is 60 mph
} obtained from Hollister (1970)

R has no units;

A = solid surface area of heliostat (include openings in solid area if they constitute less than 15 percent of the total area) (ft^2);

h = chord length of the heliostat (ft);

H = height of the center of the heliostat area from ground (ft); and

C_{Fx}, C_{Fz}, C_{My}, etc. = the respective force and moment coefficients (no units).

---

* indicates multiplication

Note: The approach flow is identical for the isolated or in-field cases, i.e. outside the field.

The equation for U assumes a wind with a relatively stable mean value and direction over at least a 10-minute period. Thunderstorm outflows of short duration, dust devils, or tornados may not have the same gust-to-mean-wind ratio. However, if the mean wind is based on $U_{gust}/1.6$ using the above equations for these wind events, then the provisions of this document might reasonably apply.

No coefficients are included for y-axis forces or for x-axis moments. In some wind-tunnel tests an attempt was made to measure these components for flat plates, but the forces and moments were sufficiently low that reliable measurements were not obtained. Since those components were never a requirement for any of the wind-tunnel tests, extra efforts were not made to obtain these values. For parabolic collectors, these forces and moments can be obtained from x-axis forces and y-axis moments by a suitable coordinate transformation.

The wind-tunnel models were mostly ideal shapes which did not include supporting trusses. The forces on the supporting trusses may, in many cases, be larger than the y-axis forces on the collectors.

All tested heliostats were nearly square in shape or were round flat discs. Both flat shapes had essentially the same load coefficients. The influence of other shapes or aspect ratios is not known from tests leading to this document.

The specific location of the hinge point about which hinge moments are defined is centered on the collector geometry and is 0.062 h from the rear surface (downwind side when beta = 0 and alpha = 90), where h is the heliostat chord or parabolic collector diameter.

EFFECTS OF ATMOSPHERIC TURBULENCE

The wind load data in this document were obtained in a boundary-layer wind tunnel in which the mean velocity and turbulence intensity variation with height were modeled. As part of the research studies, the effect of varying turbulence intensity was studied. A significant effect of turbulence intensity was found. Figures 2 and 3 show this variability. Figure 2, taken from Peterka et al. (1989), shows that load coefficients increase dramatically for turbulence intensities above 10 percent. Turbulence intensity for an open country environment on these graphs is about 15 to 18 percent. Collectors designed for a rougher environment than open country should include the increase in load coefficient from turbulence. Table 1 provides some guidance in the level of turbulence intensity expected in various exposures. Note that some of the increase in load from turbulence will be removed by lower mean wind speeds in the rougher exposures. Higher turbulence does not always mean higher loads. For example, in a dense field of collectors where mean velocities are very low and turbulence intensities are high, there is a net decrease in peak wind loads.

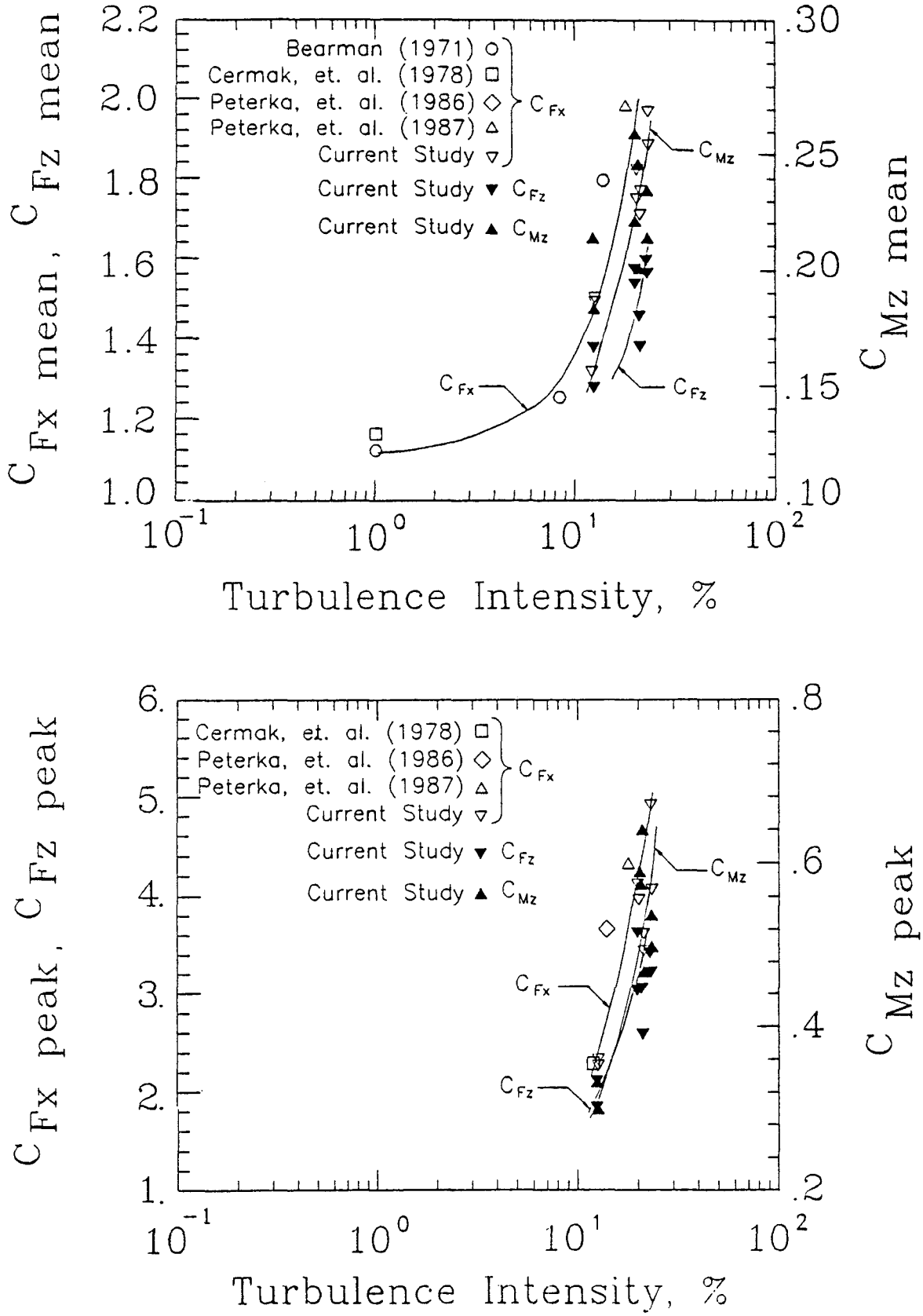

Figure 2. Variation of C_{Fx}, C_{Fz} and C_{Mz} with turbulence intensity for an isolated heliostat.

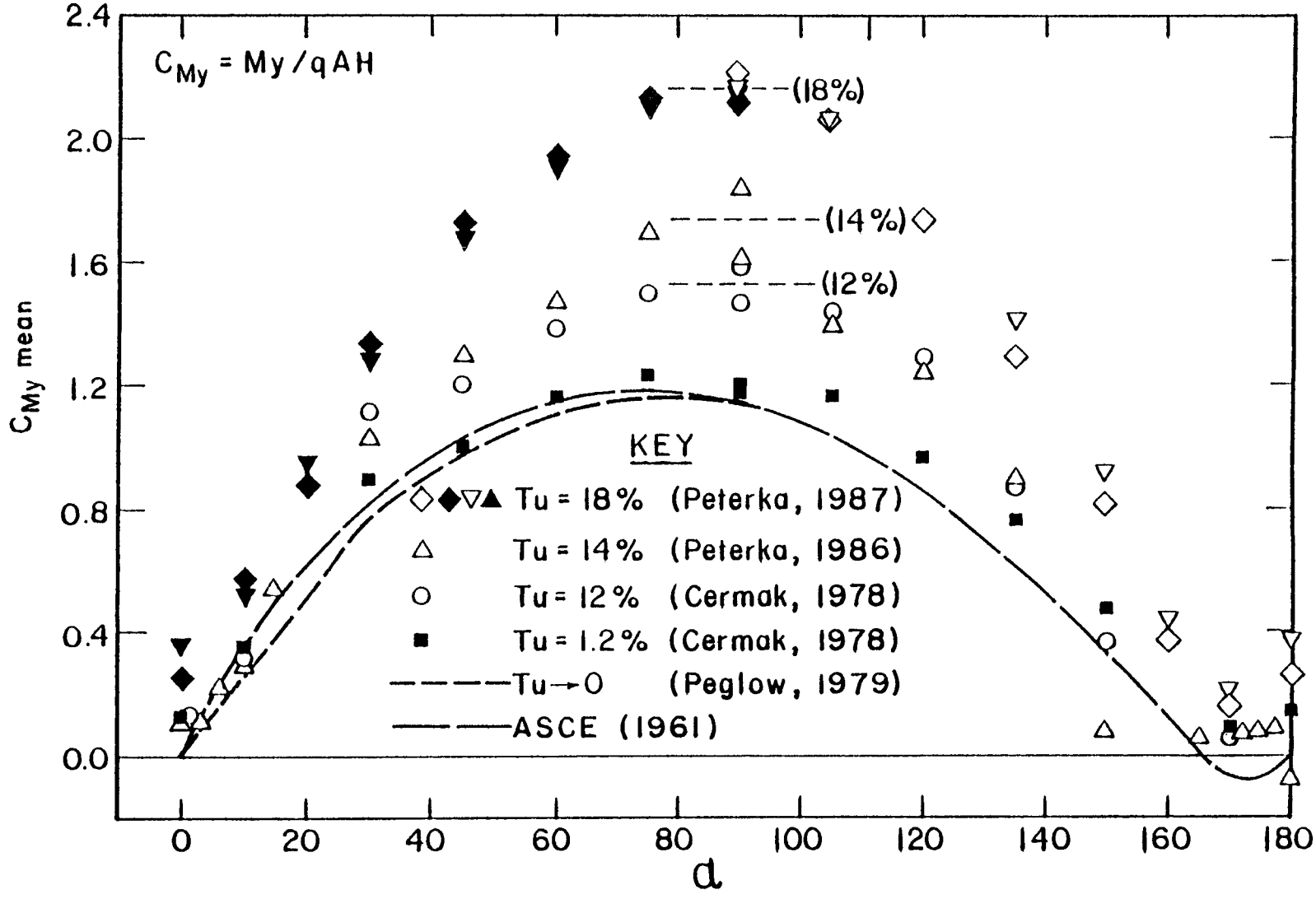

Figure 3. Variation of mean C_{My} with elevation angle and turbulence intensity.

Figure 3 is also taken from Peterka et al. (1989). It shows the variation of base moment C_{My} with elevation angle alpha. The solid line represents ASCE (1961) which was based on wind-tunnel data obtained with near-zero turbulence intensity and no mean velocity variation with height. The dashed line in the figure is data obtained by Peglow (1979) on a full-scale 20 x 20 foot heliostat installed in the 40 x 80 foot wind tunnel at NASA Ames Research Center. This wind-tunnel test also had a near-zero turbulence intensity. Comparison to the ASCE (1961) data is excellent. The solid squares in Figure 3 show base moment coefficients on a Colorado State University heliostat model placed in a 1.2 percent turbulence intensity in a boundary-layer tunnel in which the atmospheric simulation was removed from the tunnel. The comparison with both 1961 ASCE and Peglow data is good - the CSU measurements are slightly higher than the two near-zero turbulence cases due to the low, but non-zero, level of turbulence in the CSU tunnel. Three other data sets in Figure 3 show the influence of increasing turbulence in a CSU boundary-layer simulation (which also included the variation of mean velocity with height) on base moment. The variation of load coefficient with turbulence was not an effect of the mean velocity variation with height since this variation was the same in the 12, 14 and 18 percent turbulence cases.

The conclusion based on these data is that atmospheric turbulence significantly increases wind loads on solar collectors and cannot be ignored. Data based on low-turbulence tests, such as those typically obtained in aeronautical-type wind tunnels and in ASCE (1961), is not appropriate for solar collector design.

LARGEST WIND LOADS ON ISOLATED COLLECTORS - Heliostats and Parabolic Dishes

Table 2 presents the largest mean and peak wind force and moment coefficients as a function of wind direction, β, and collector tilt, α, for a flat (or nearly flat) rectangular or circular heliostat alone in an open-country atmospheric wind. Table 3 presents the same information for an isolated parabolic dish collector. Note that the maximum drag force and maximum base overturning moment occur at the same α and β as might be expected for both the heliostat and the parabolic dish. Less intuitively, the maximum lift force and maximum hinge moment occur at the same α and β for the heliostat. Stow loads have been included in Tables 2 and 3. Stow load coefficients are small but are usually used with higher survival wind speeds. The total vector force acting on a heliostat acts almost parallel to the normal to the collector surface. This indicates a small component of force in the plane of the collector (wind-tunnel collectors had minimal truss supporting structure). Where MH_y is largest, the heliostat normal force is non-uniform with largest (but unknown) value near the upwind edge.

LOAD COMBINATIONS FOR ISOLATED HELIOSTATS AND PARABOLIC DISHES

Load combinations at conditions other than those where one component is a maximum (which are tabulated in the previous section) are useful for design. Mean and peak load coefficients for heliostats for a range of elevation angle α and wind direction β are shown in Figures 4 to 7. Similar coefficients for parabolic dishes with depth-to-diameter ratio of 0.1 (f/D = 0.625) are shown in Figures 8 to 15.

Some guidance is helpful in the use of Figures 4 to 15:

1. Uncertainty in portions of graphs is significantly higher than for the data in Tables 2 and 3. The number of experiments in most

Table 2. **HELIOSTATS** -- Wind load coefficients on isolated heliostats when one component is a maximum.

	Fx, My Max	Fz, MHy Max	Mz Max	Stow Loads
PEAK LOADS				
α, degrees	90	30	90	0
β, degrees	0	0	65	0
Fx	4.0	2.1	3.7	0.6
Fz	1.0	2.8	0.5	0.9
MHy	0.25	0.6	0.15	0.2
Mz	0.29	0.06	0.7	0.02
MEAN LOADS				
α, degrees	90	30	90	0
β, degrees	0	0	65	0
Fx	2.0	1.0	1.6	0.1
Fz	0.3	1.35	0.3	0.1
MHy	0.02	0.25	0.02	0.02
Mz	0	0	0.25	0

n = 0.15 Tu = 18% Zo = 0.03 meters

Table 3. **PARABOLIC DISHES** -- Wind load coefficients on isolated parabolic dishes when one component is a maximum.

	Fx Max	Fz Max	MHy Max	Mz Max	Stow Loads
PEAK LOADS					
α, degrees	90	30	60	90	0
β, degrees	0	0	180	60	0
Fx	3.5	1.9	-1.8	3.03	0.33
Fz	0.31	3.1	0.8	0.33	0.98
MHy	0.31	0.25	0.35	0.35	0.22
Mz	0.15	0.06	.08	0.35	0.02
MEAN LOADS					
α, degrees	90	30	60	90	0
β, degrees	0	0	180	60	0
Fx	1.75	1.1	-1.0	1.32	0.13
Fz	0.17	1.7	0.5	0.09	0.1
MHy	0.11	0.13	-0.17	0.14	0.09
Mz	0	0	0	0.13	0

n = 0.15 Tu = 18% Zo = 0.03 meters

Note: All data in Table 3 is for a parabolic dish shape with depth to diameter ratio of 0.1 (f/D = 0.625).

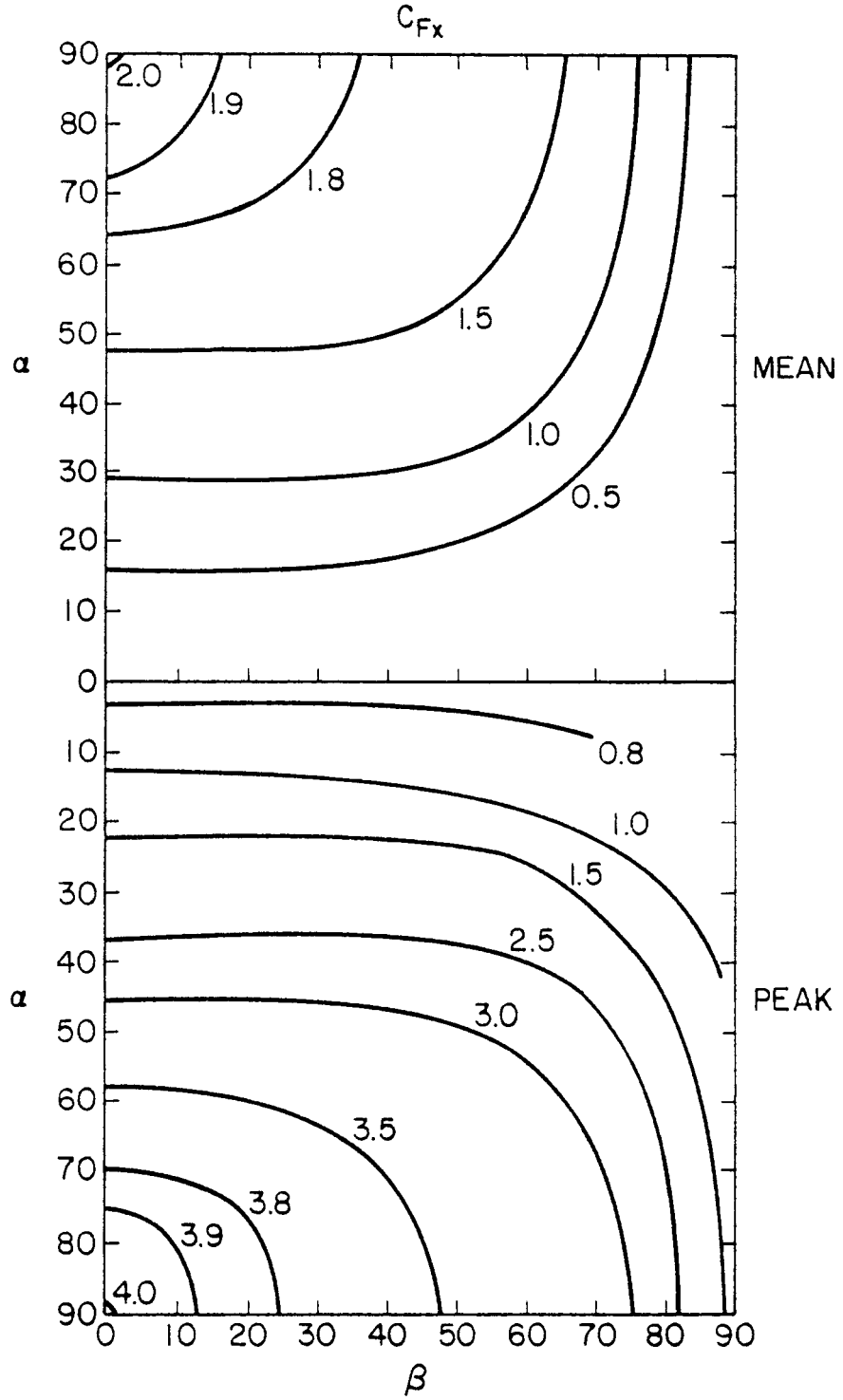

Figure 4. Drag force coefficients C_{Fx} for the heliostat.

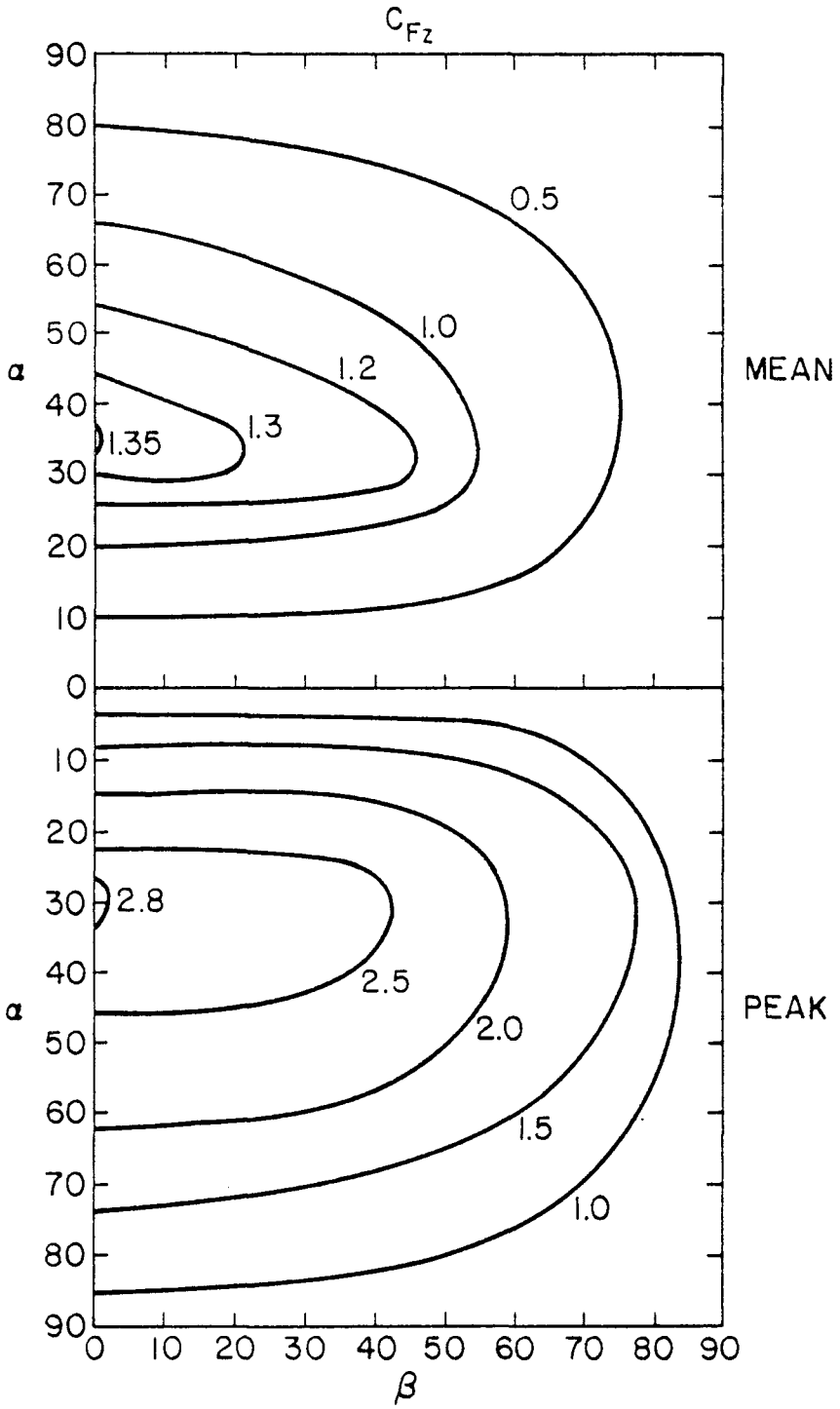

Figure 5. Lift force coefficients C_{Fz} for the heliostat.

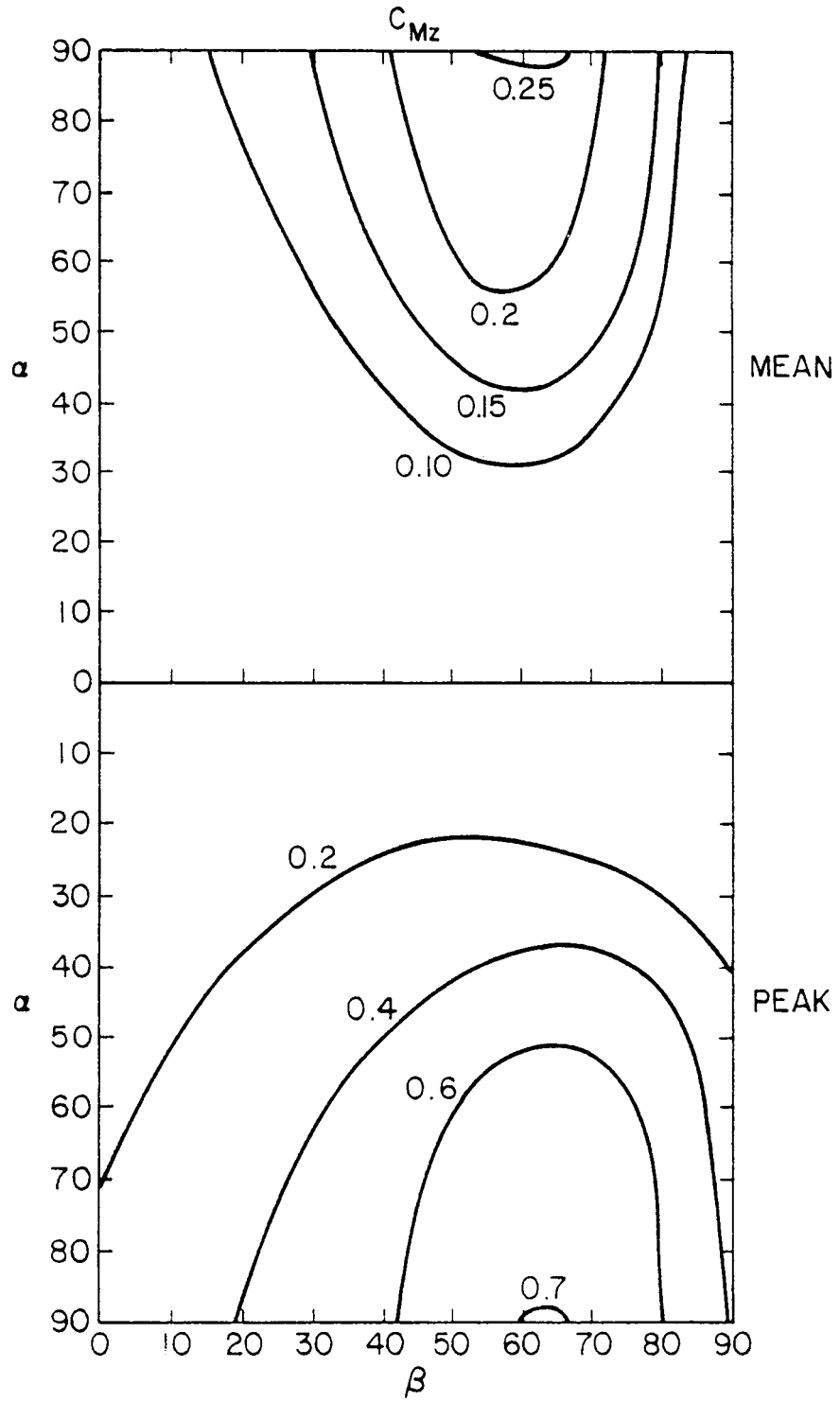

Figure 6. Azimuth moment coefficients C_{Mz} for the heliostat.

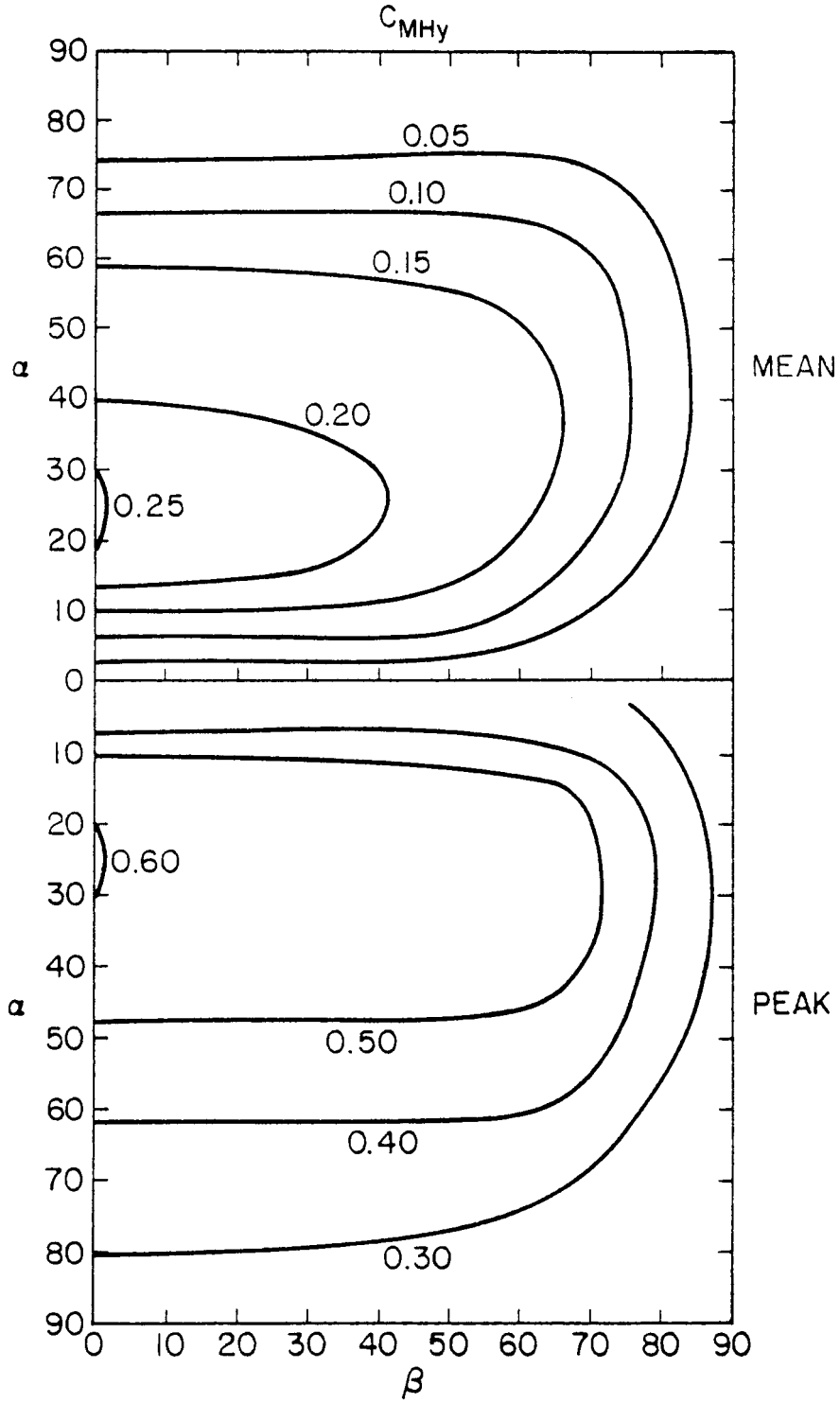

Figure 7. Hinge moment coefficients C_{MHy} for the heliostat.

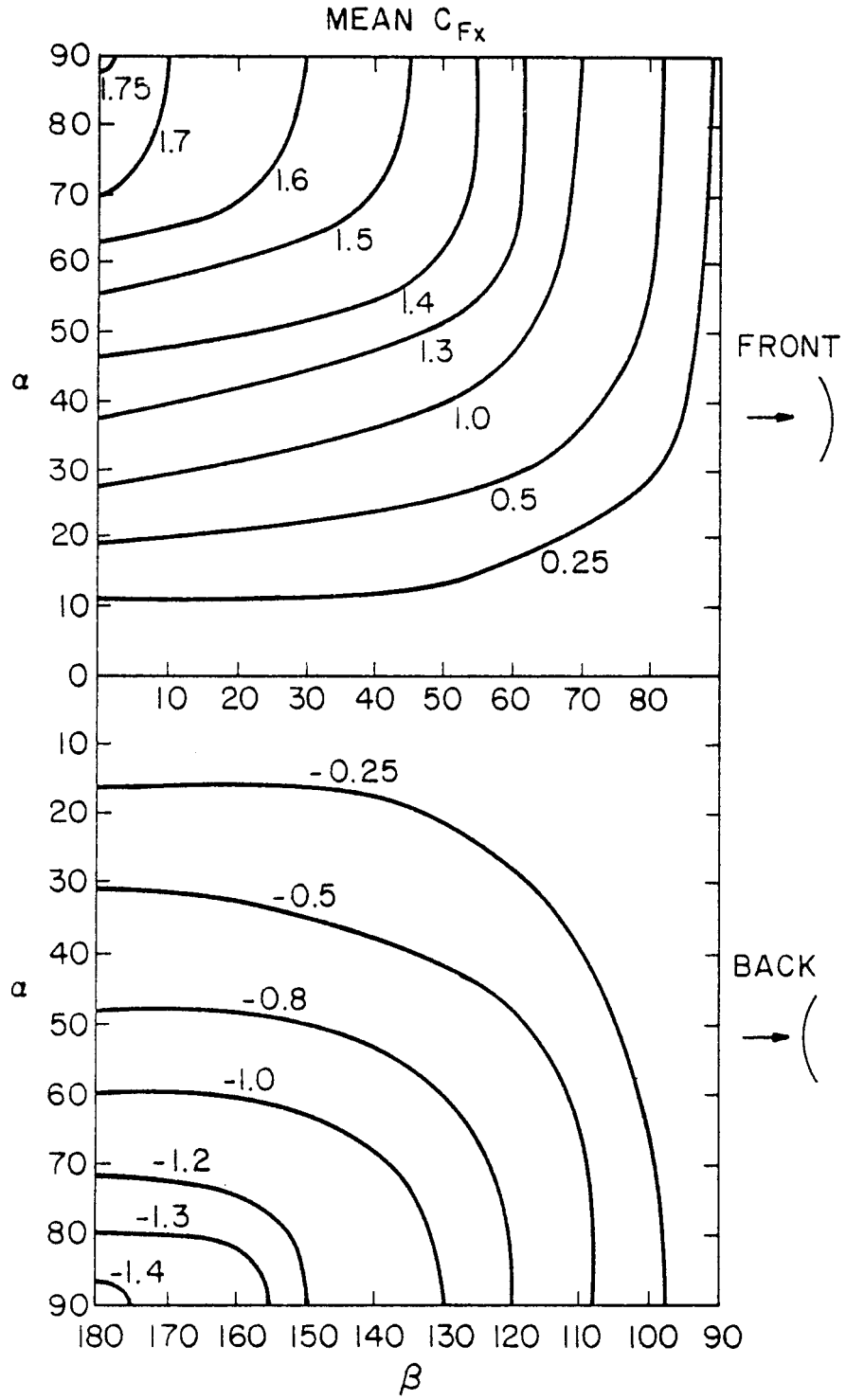

Figure 8. Mean drag force coefficients MEAN C_{Fx} for the parabolic dish.

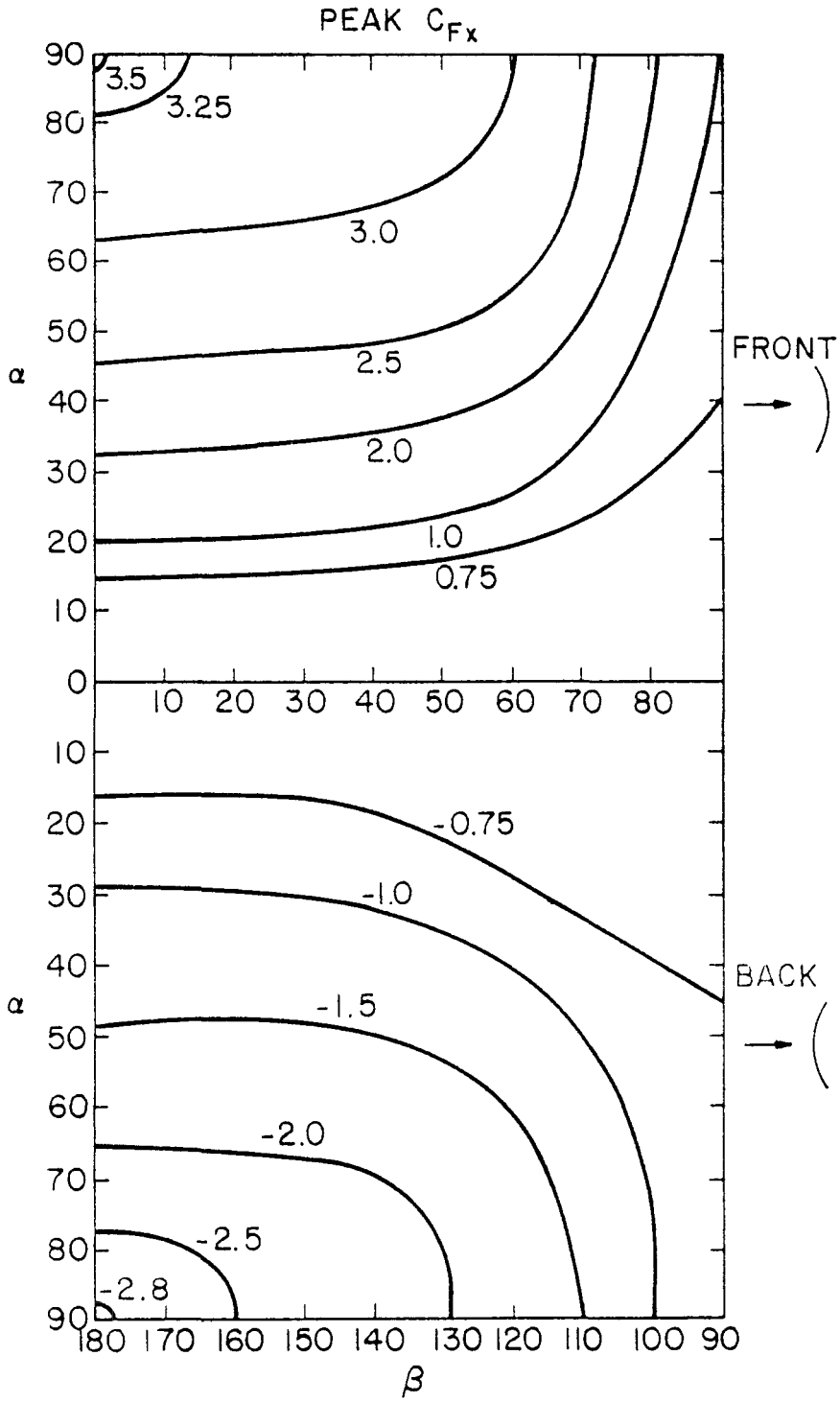

Figure 9. Peak drag force coefficients PEAK C_{Fx} for the parabolic dish.

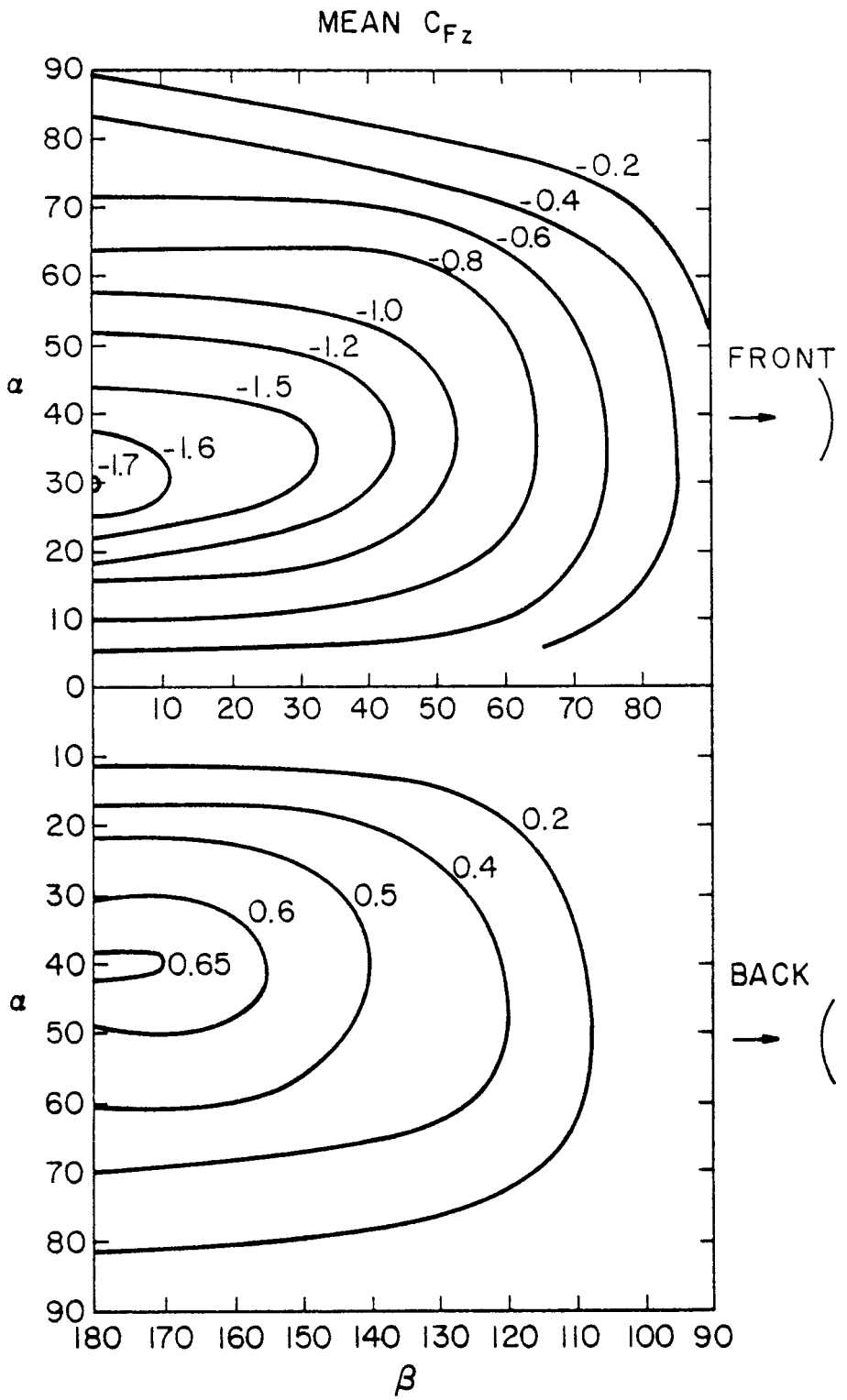

Figure 10. Mean lift force coefficients MEAN C_{Fz} for the parabolic dish.

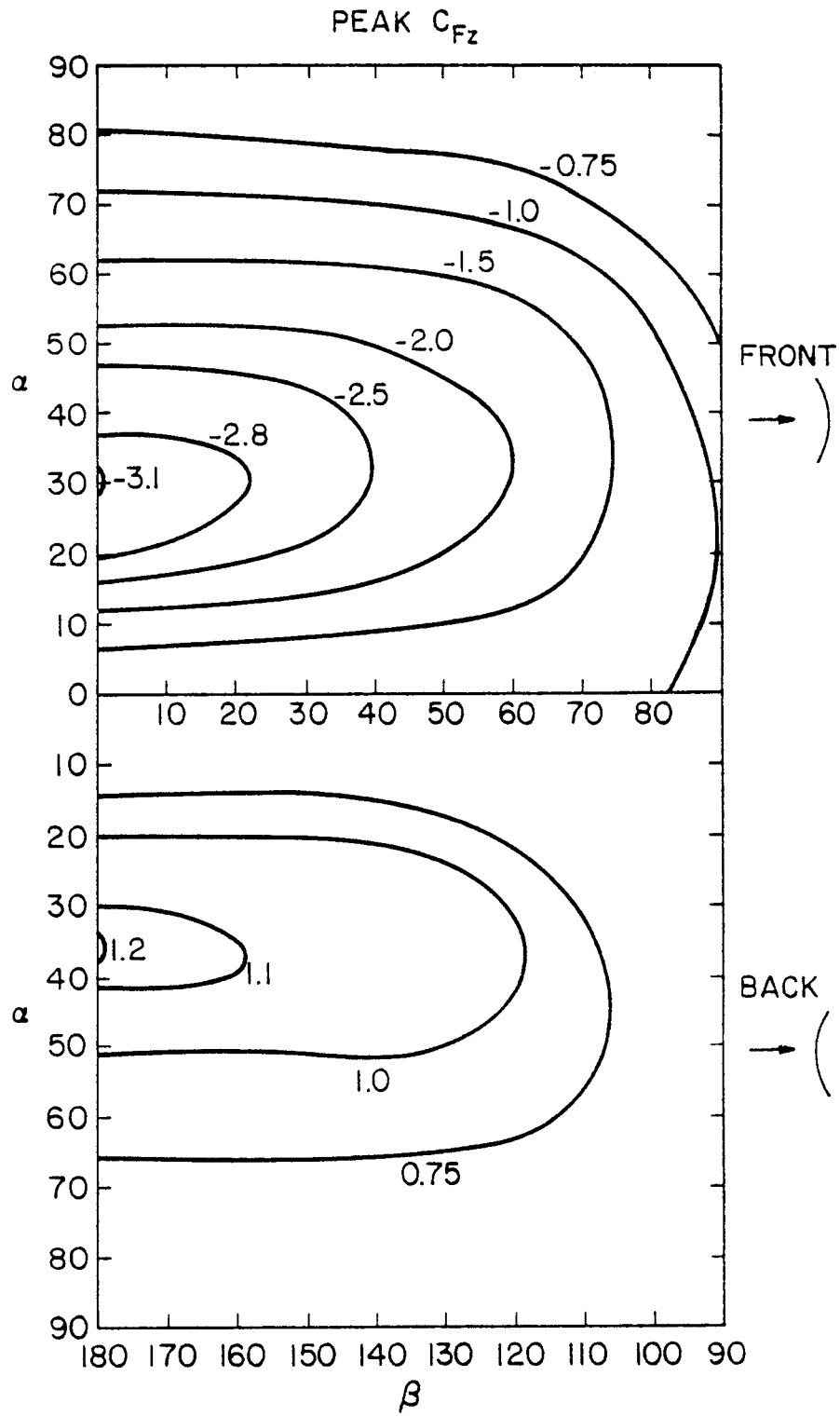

Figure 11. Peak lift force coefficients PEAK C_{Fz} for the parabolic dish.

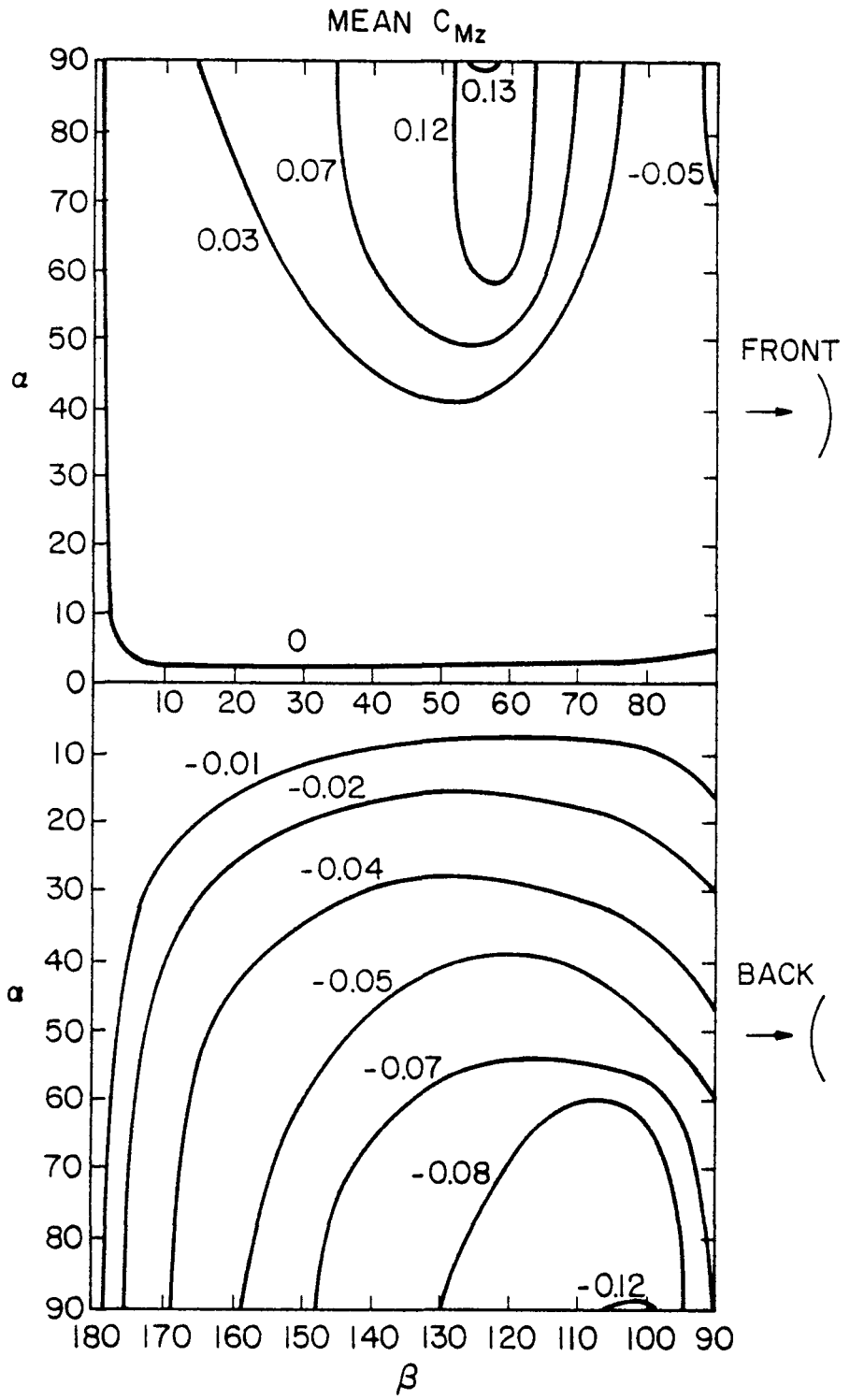

Figure 12. Mean azimuth moment coefficients MEAN C_{Mz} for the parabolic dish.

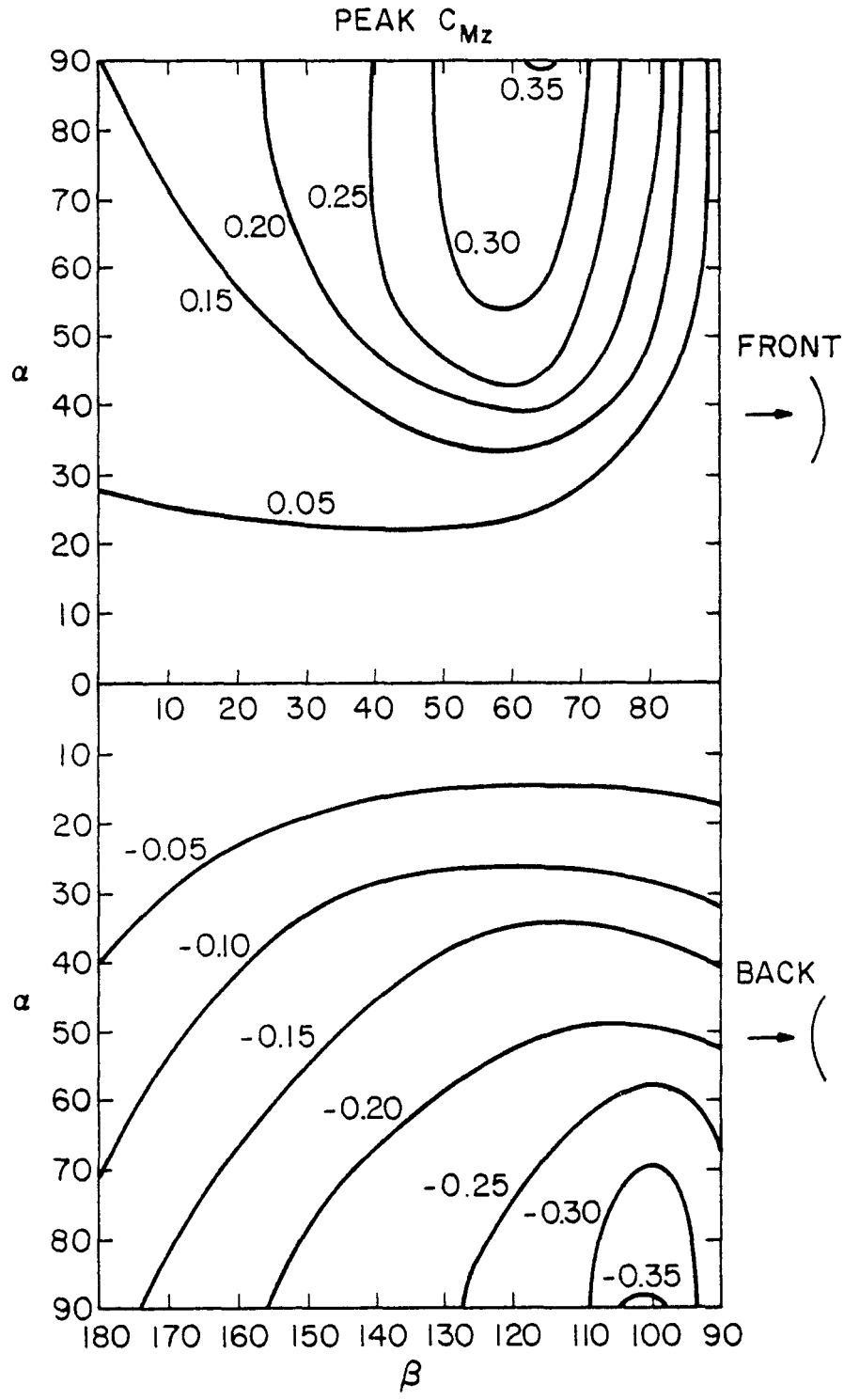

Figure 13. Peak azimuth moment coefficients PEAK C_{Mz} for the parabolic dish.

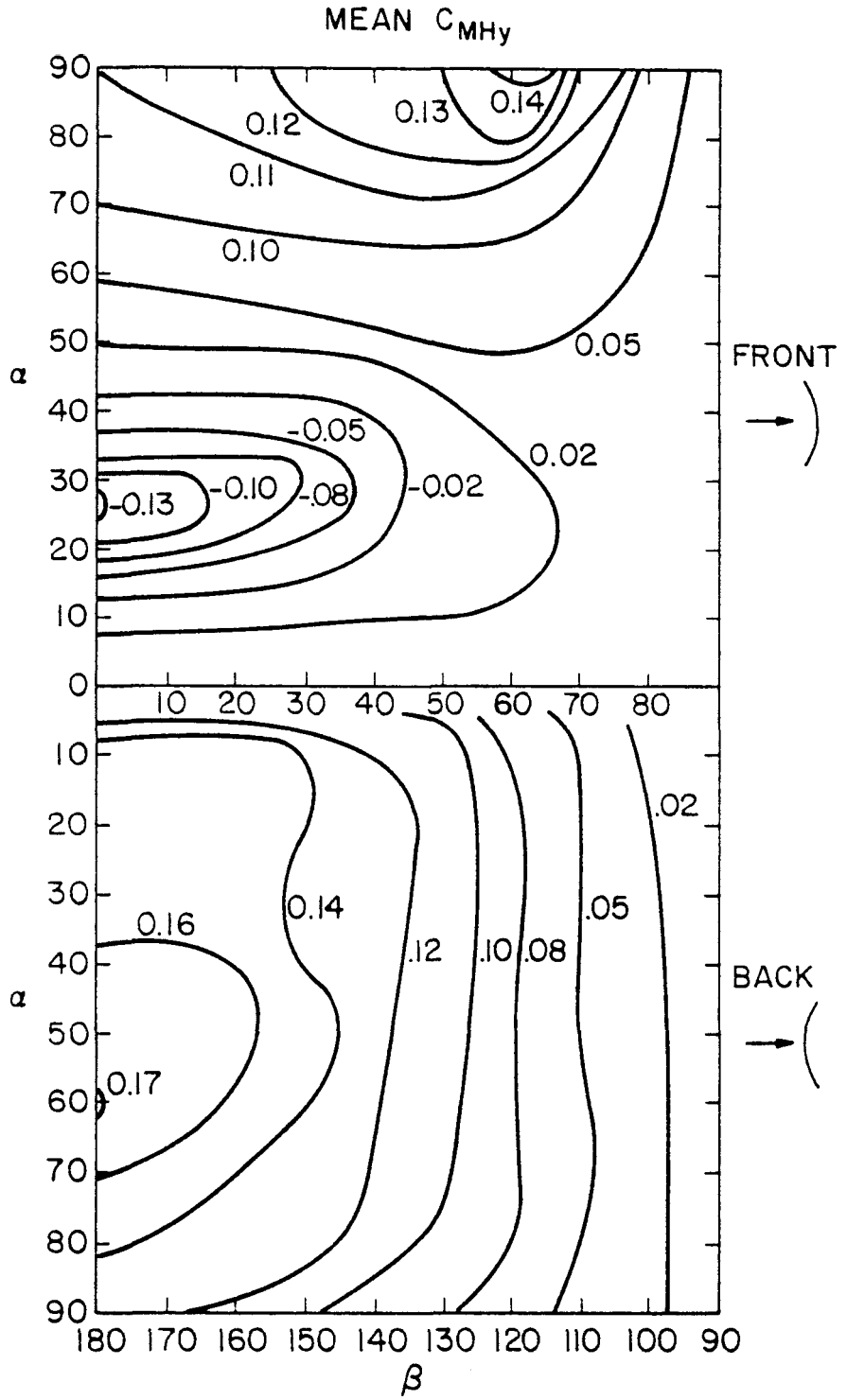

Figure 14. Mean hinge moment coefficients MEAN C_{MHy} for the parabolic dish.

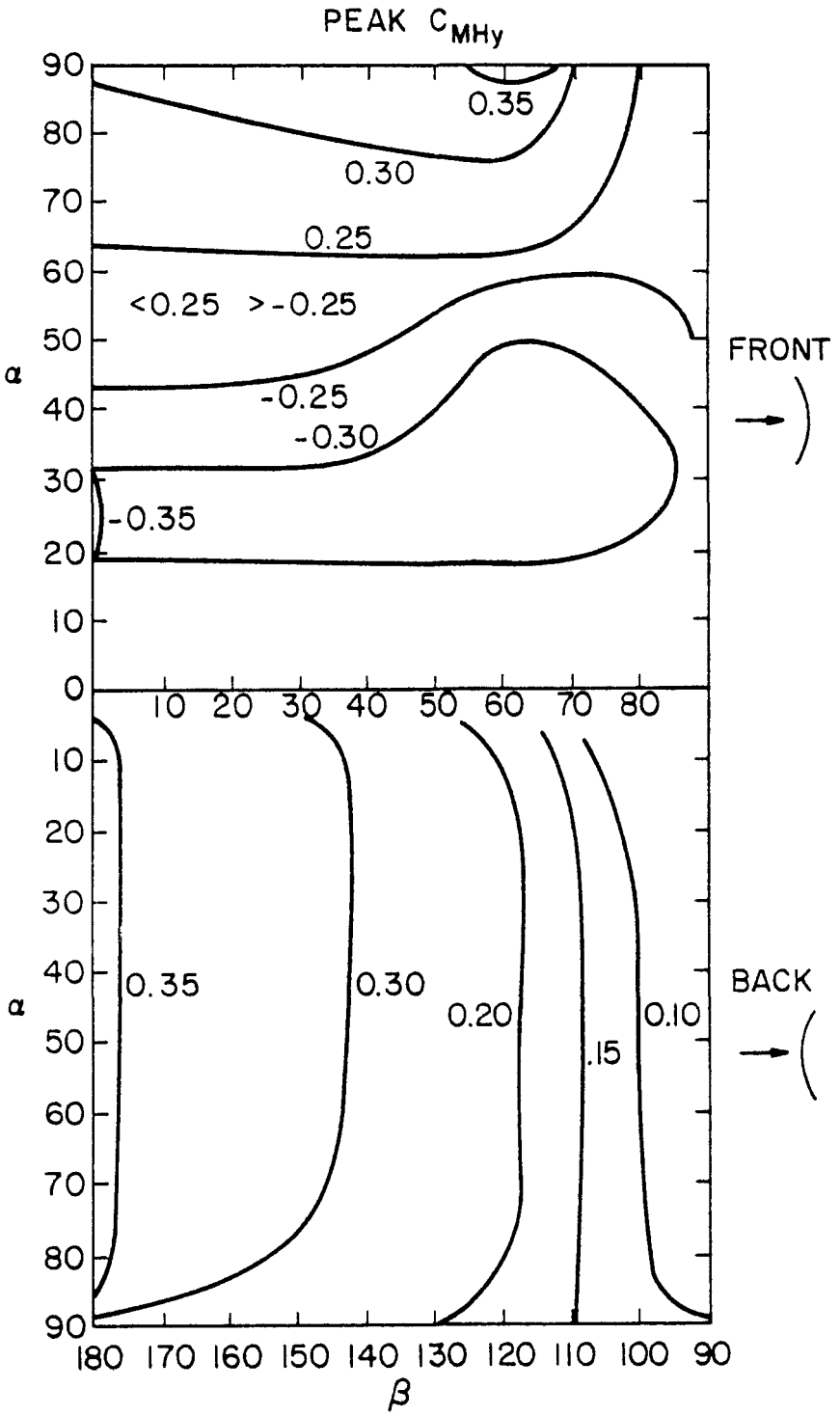

Figure 15. Peak hinge moment coefficients PEAK C_{MHy} for the parabolic dish.

low-coefficient-magnitude areas of the graphs is not as large as those near maxima where the wind-tunnel data was concentrated. The range of uncertainty is difficult to quantify, since no field measurements are available for comparison and since the sensitivity to wind turbulence is high as shown in Figure 2. Parabolic dish loads have a smaller uncertainty than heliostats. As a rough guide heliostat (parabolic dish) coefficients probably have an uncertainty of 15-20 (10-15) percent of the largest values in each graph.

2. The heliostat loads of Figures 4 to 7 for $90 < \beta < 180$ were folded onto the 0 - 90 degree range since the loads are nearly symmetric about $\beta = 90$ degrees when the heliostat has no supporting truss work. For this reason, the load coefficients do not have signs. To determine signs, referring to Figure 1, the sign of Fx is positive for $\beta < 90$ and negative for $\beta > 90$. Fz is negative when the wind impinges on the upward surface, positive when the wind hits the lower side. The sign of all heliostat moments is such that the wind action tries to force the collector toward a maximum drag orientation with the wind impinging directly on its face.
3. The parabolic dish loads of Figures 8 to 15 are presented separately for $\beta < 90$ (called FRONT in the figures) and for $\beta > 90$ (called BACK). Coefficient signs are placed directly on the graphs. For some graphs (for example, Figure 15), the sign of the peak changes suddenly from positive to negative. This occurs when the absolute value of the negative peak moment becomes larger than the magnitude of the positive peak load.

LOCAL PRESSURE DISTRIBUTION

The distribution of local mean or peak pressures over the surface of collectors cannot be determined unambiguously from the total forces and moments presented in previous sections. There is an infinite set of pressure distributions which can be integrated over the collector surface to obtain the recorded forces and moments. The research studies leading to this design method were directed toward integrated loads, and so pressure distributions were measured in only one study involving parabolic dishes. Insufficient local pressure distributions on heliostats have been measured for general use.

Figures 16 to 23, taken from Peterka et al. (1990), show mean pressure distributions on an isolated solid parabolic collector at a variety of orientations. The defining equation for mean pressure in terms of the pressure coefficients in the figures are:

$$\underline{\text{Mean Pressure}}: \quad P = C_p * Q. \tag{7}$$

In each figure, the concave face is displayed above the convex face. Contours on the concave face correspond to the viewer looking directly at that face, while the contours on the convex face are viewed from the concave side through the collector as if the concave face were invisible. Thus the viewer can readily make a correspondence between values on the opposing surfaces of the collector. Since the pressure taps were not placed on the collector edge, the inner ring in the figures corresponds to the maximum radius of tap placement. The space between the inner and outer rings in the figures represents the area on the collector surface for which pressures were not measured.

Peak pressures were measured on the parabolic dish collectors but have not been presented in plots in Peterka et al. (1990). The largest values of peak pressure coefficient were +2.6 and -5.9. These occurred for the same

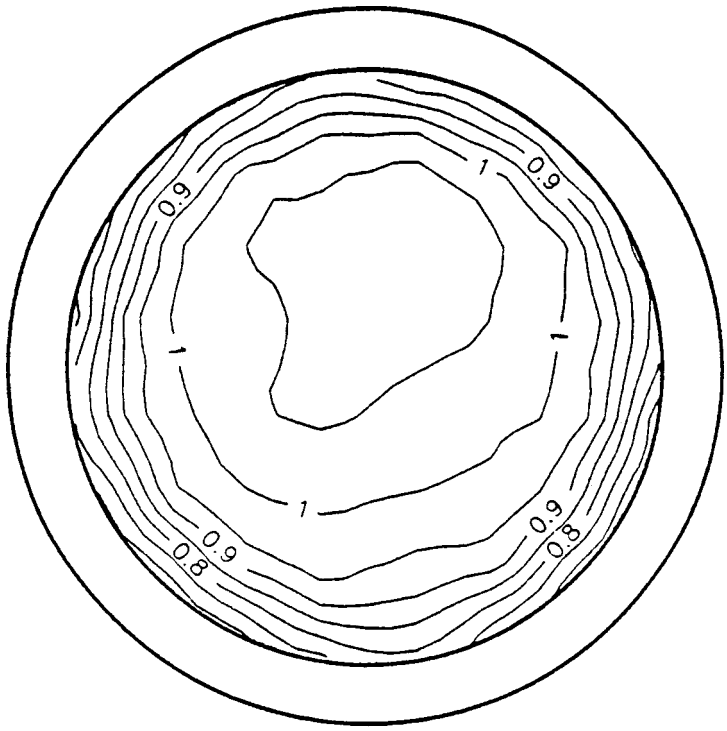

(a) concave face (windward)

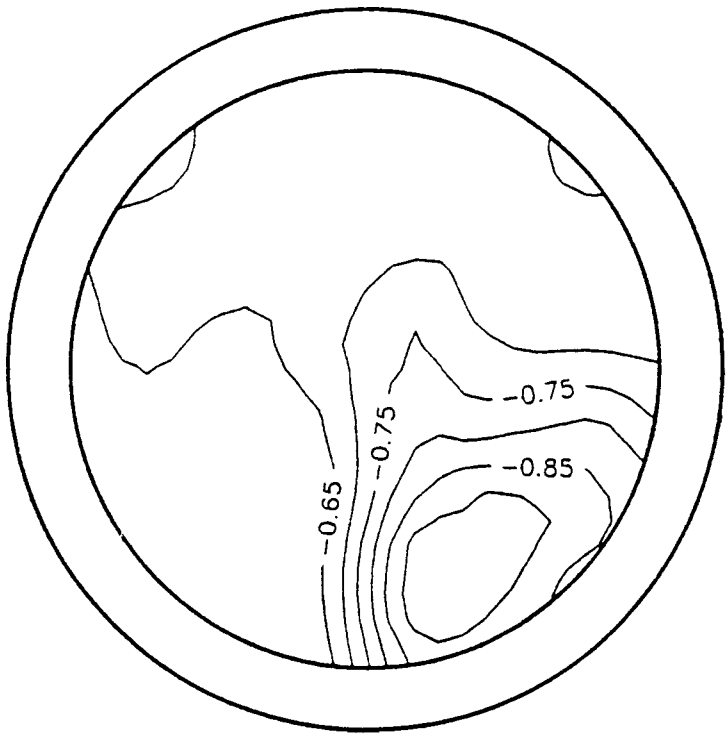

(b) convex face (leeward)

Figure 16. Mean pressure coefficients (α = 90 and β = 0).

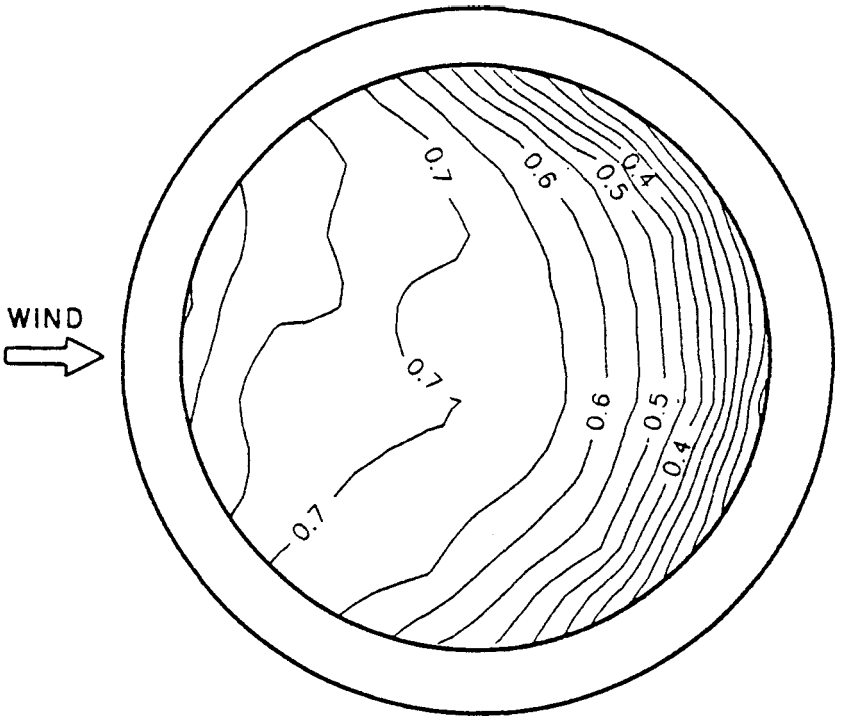

(a) concave face (windward)

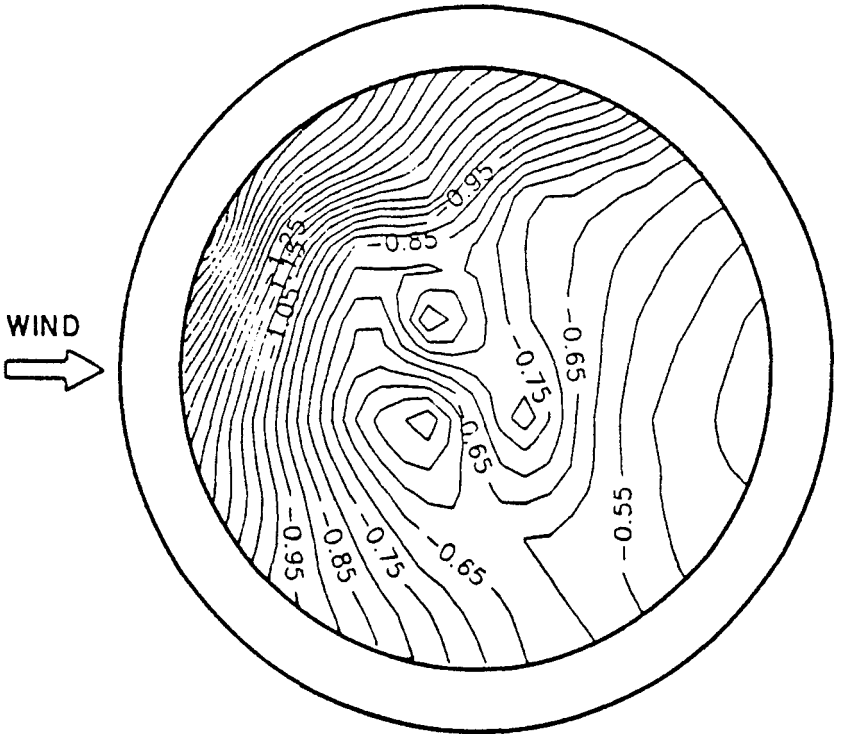

(b) convex face (leeward)

Figure 17. Mean pressure coefficients (α = 90 and β = 60).

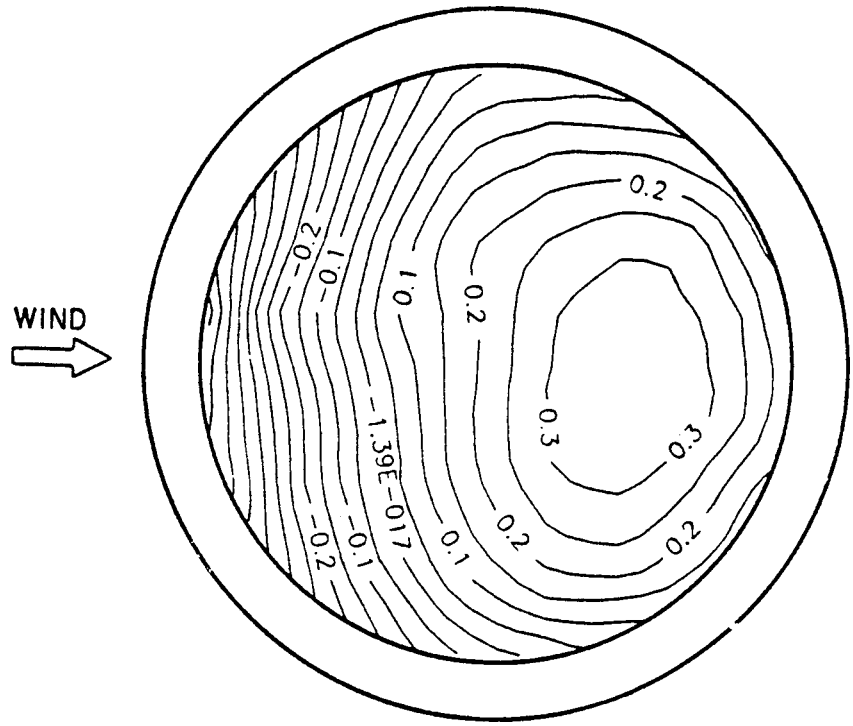

(a) concave face

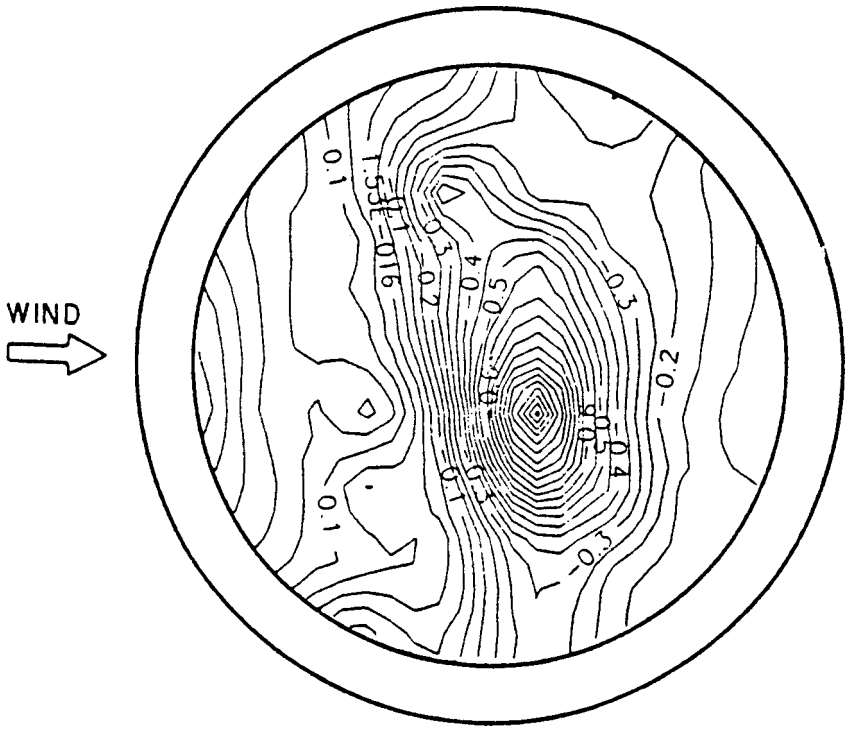

(b) convex face

Figure 18. Mean pressure coefficients (α = 90 and β = 90).

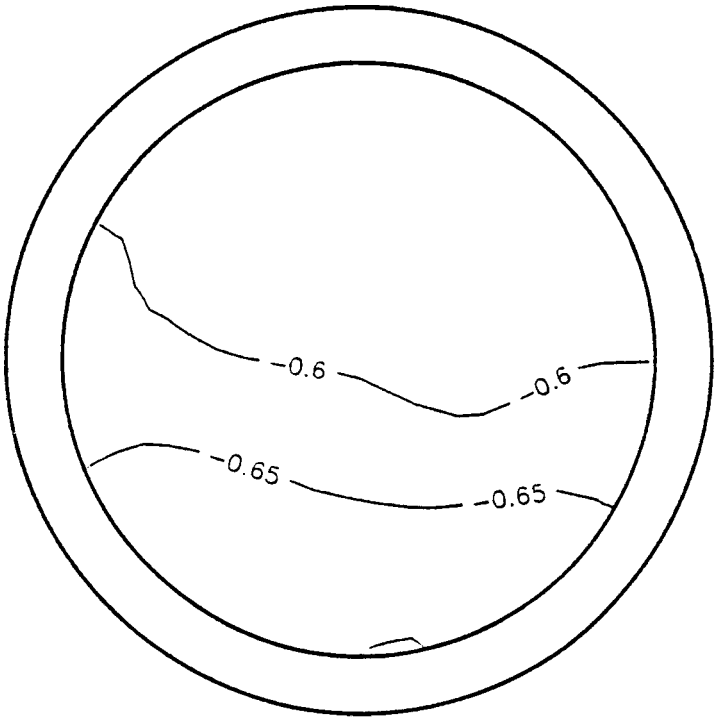

(a) concave face (leeward)

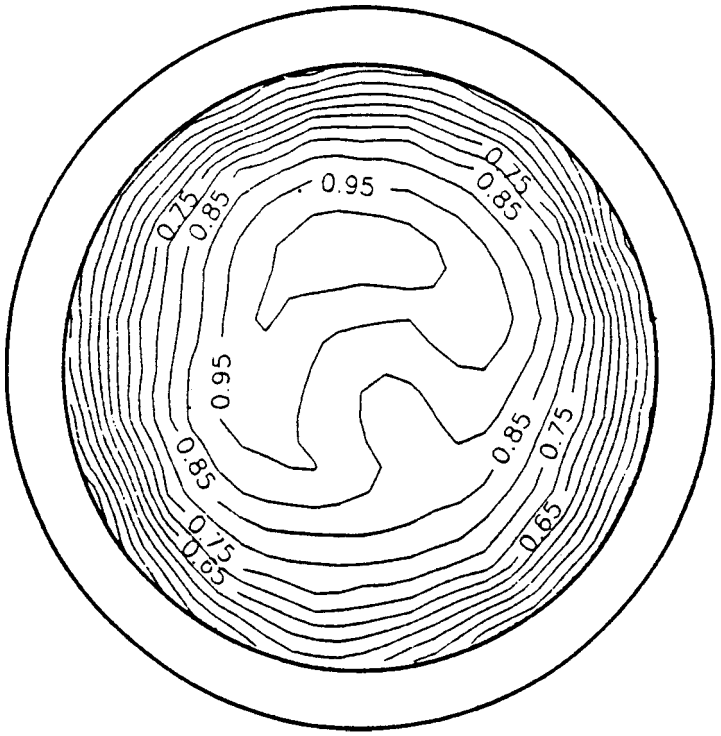

(b) convex face (windward)

Figure 19. Mean pressure coefficients (α = 90 and β = 180).

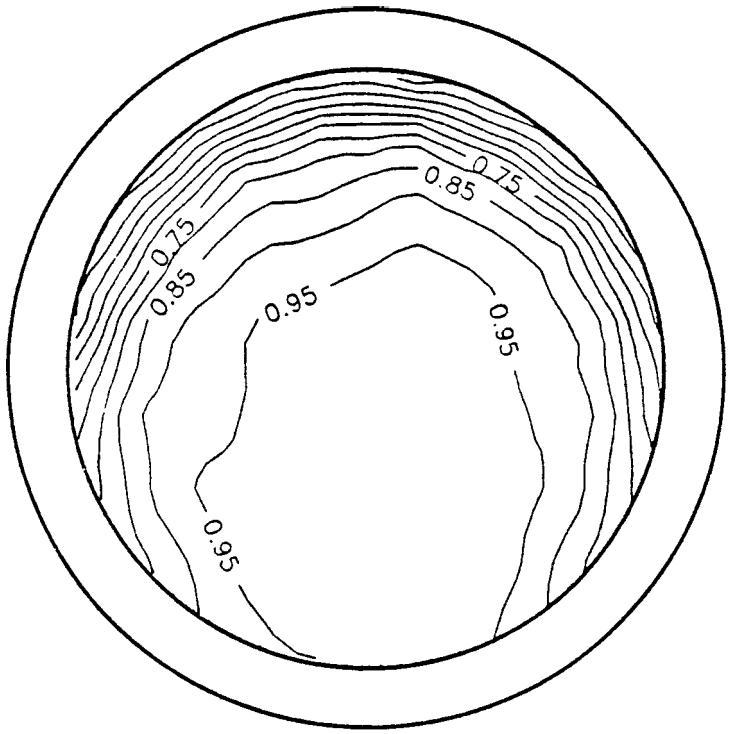

(a) concave face (windward)

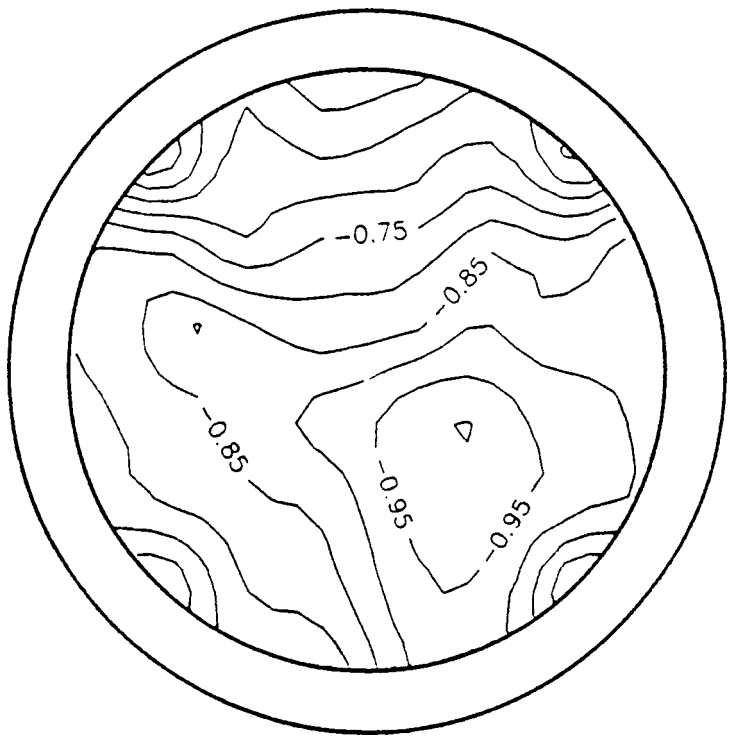

(b) convex face (leeward)

Figure 20. Mean pressure coefficients (α = 60 and β = 0).

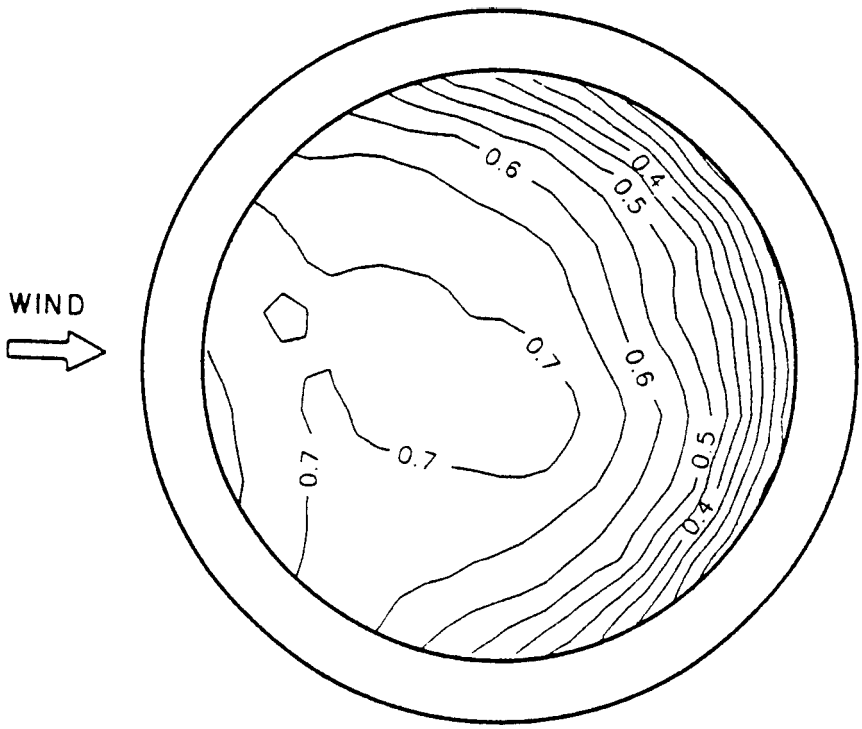

(a) concave face (windward)

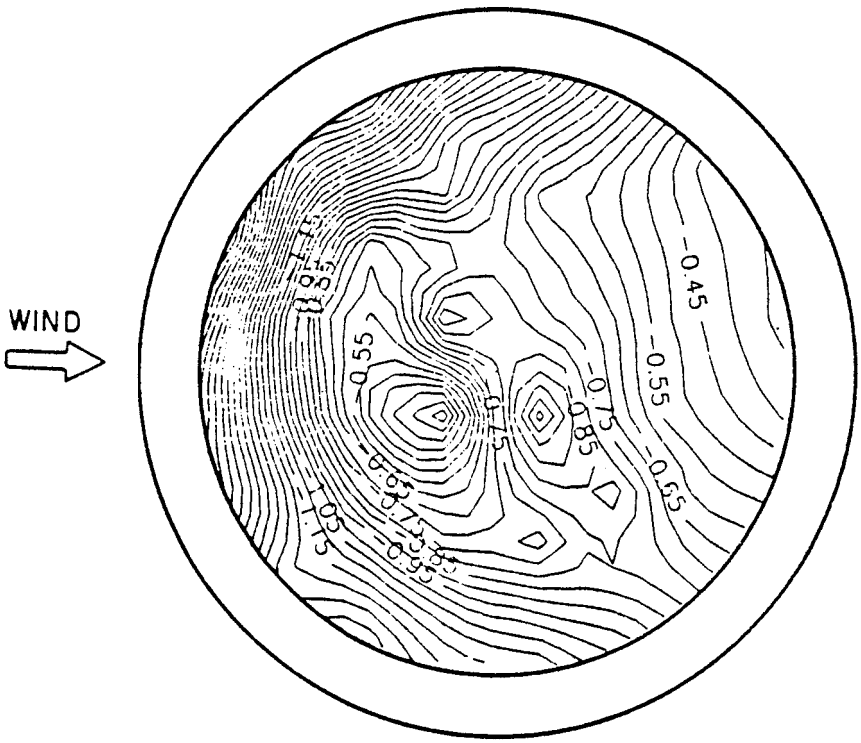

(b) convex face (leeward)

Figure 21. Mean pressure coefficients (α = 60 and β = 60).

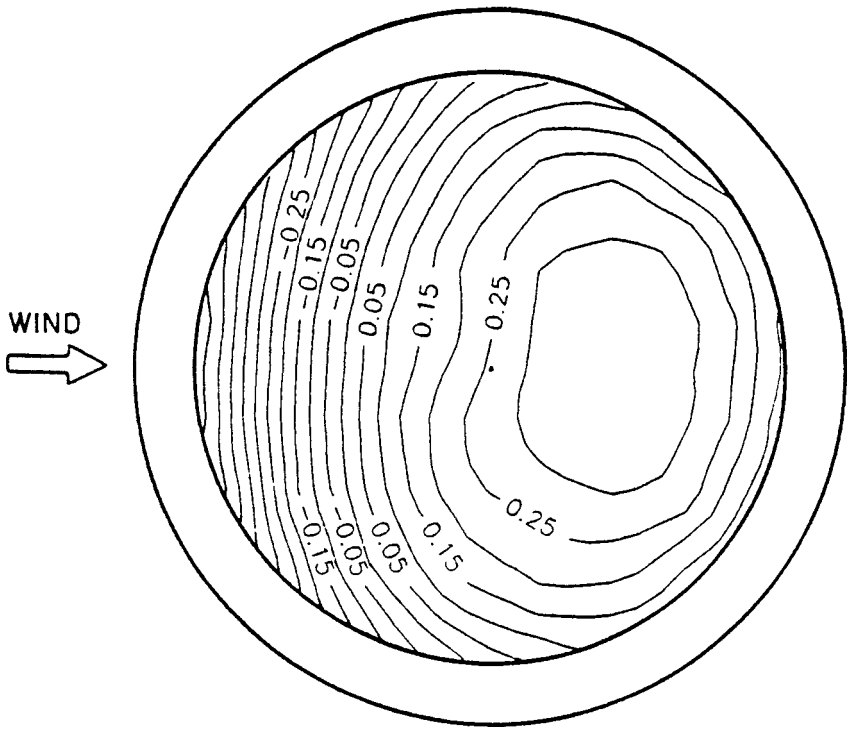

(a) concave face

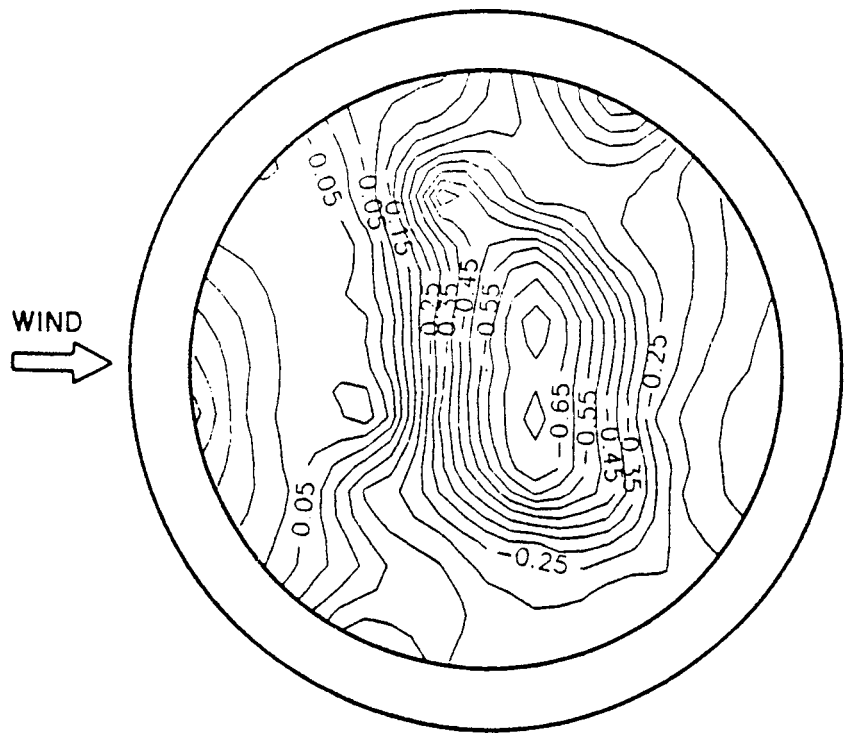

(b) convex face

Figure 22. Mean pressure coefficients (α = 60 and β = 90).

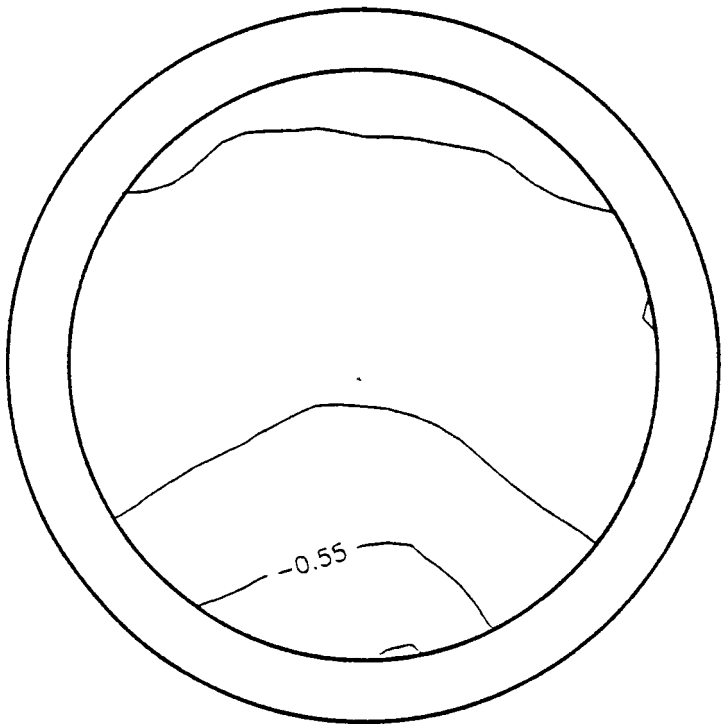

(a) concave face (leeward)

(b) convex face (windward)

Figure 23. Mean pressure coefficients (α = 60 and β = 180).

orientations which gave the largest mean coefficients (shown in Figures 16 to 23) of +1.1 and -2.1. Peak pressure differences across the collector must be measured directly to be valid; these were not part of that research program.

MAXIMUM WIND LOADS ON COLLECTORS IN A FIELD - General Blockage Area

This section may be used when calculating maximum loading on heliostats and parabolic collectors as part of a field for a given load component. For loads not at their maximum, insufficient data is available to reliably use this section and the following section should be used.

A convenient parameter correlating to the wind loading of an in-field collector is its Generalized Blockage Area or GBA that is defined as

$$GBA = \frac{\text{Solid area of upwind blockage projected to wind direction}}{\text{Area of ground occupied by the blockage objects}}. \tag{8}$$

The GBA includes the effects of wind fences and upwind collectors.

The calculation of the GBA can be a cumbersome task using the above general definition since the wind direction, β, relative to the collector, the collector tilt, α, and the angle of the wind relative to a wind fence must be taken into consideration in determining the area projections of the various blockage elements upwind of a particular in-field collector unit. Therefore a simplified method for GBA calculation has been developed that uses a factor, K, to correspond to the maximum loads for each component of loading. We redefine the GBA as

$$GBA = \frac{(K)(AH) + AS}{AF} \tag{9}$$

where

AH is the actual surface area of the collectors (chord times width for a rectangular unit; πh^2 for a parabolic unit) in the AF;

AF is the representative ground area occupied by the collectors;

AS is the solid area of fences (external and internal) within AF; and

K is a factor to account for elevation and azimuth angle of collector for maximum loading for a given force or moment component;

in which the factor K has the following values:

Component	K
F_x	1.0
F_z	0.5
M_{Hy}	0.5
M_z	0.5

Figure 24 illustrates the layout for a simplified GBA calculation for five unit locations, rows 1 through 5. It is not necessary for the user to know the wind direction or collector tilt in performing the simplified GBA calculation, because that knowledge is implicit in the factor K.

The treatment of collector units in rows 1 through 4 should be self-evident from the figure. Collectors denoted by a square, solid symbol within each representative field ground area are included in the calculation of AH in the simplified GBA equation, Eq. (9). Note that a unit in the fifth row is treated differently from the other cases. By the fifth row, an external wind fence is no longer an effective blockage element (by the fourth row for a denser field of collectors). Therefore the representative field ground area, AF, for a collector in the fifth row is reduced as shown in Figure 24.

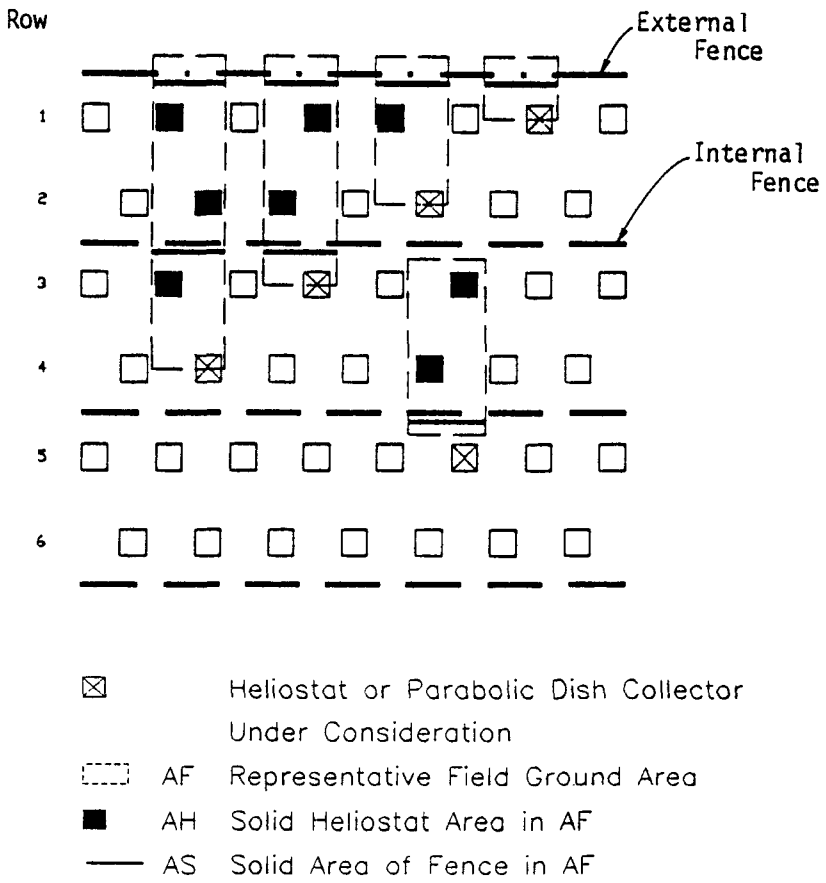

Figure 24. Layout for simplified GBA calculations for collector units in rows 1 through 5.

Field density is an issue of significant importance in designing heliostats and parabolic dishes. Research has shown two separate regimes of in-field unit performance for field densities delimited by a GBA value of 0.15 to 0.2.

(A) If the GBA $\leq$ 0.15 to 0.2, wind loads on in-field units actually increase in the first two or three rows from the edge of the field. Percentage increases are larger for peak loads than for mean loads. External wind fences will abate this effect significantly. If the field is quite sparse (i.e. GBA < 0.1 - 0.15), internal wind fences may be used to increase GBA and lower wind loads on units interior to the field.

(B) If the GBA > 0.15 to 0.2, wind loads on in-field units will decrease with row placement from the perimeter. However, an external fence will still have a significant beneficial effect on reducing wind loads on the perimeter collectors and on those up to three rows into the field. By the fourth row, unit performance is the same with or without an external fence. Internal fences have negligible effect and therefore are not recommended for in-field cases with the GBA > 0.2.

Note: If a fence is to be used in the calculation of GBA, credit for blockage area can only be obtained for wind directions within 60 degrees of perpendicular to the fence. Wind fences should be no more than 30-50 percent porosity and at least 1.15 to 1.3 H tall for maximum beneficial shielding. These conditions must be met for proper use of this data.

The following special conditions hold for calculating the GBA with Eq. (9):

(a) GBA = 0.01 for row 1 with no external fence;

(b) GBA = 0.02 for row 2 with no external fence;

(c) calculation for rows 6, 7, etc. are the same as for row 5 when the basic field density corresponds to a GBA $\leq$ 0.15 - 0.2; and

(d) calculation for rows 5, 6, etc. are the same as for row 4 when the basic field density corresponds to a GBA > 0.2.

The wind load within a field is calculated using the curves in Figures 25 through 28 for heliostats and Figures 29 through 32 for parabolic dishes. Curves are given for both mean and peak loads. The calculated GBA is used for the abscissa.

MAXIMUM COEFFICIENTS FOR IN-FIELD HELIOSTATS AND PARABOLIC DISHES

The force and moment coefficients for a heliostat placed in an array of collectors are given in Figures 25 through 28. Coefficients are a function of the Generalized Blockage Area (GBA). The in-field parabolic dish coefficients are presented in Figures 29 through 32. The thin solid lines shown in the figures represent upper bound values determined by wind-tunnel tests. All in-field cases fell on or below these lines. The thick vertical solid lines in some graphs show the highest GBA values for which data exist.

The dotted lines in the figures denote GBA values separating the thin line segments and serve as an aid to the user in calculating the appropriate force or moment coefficient. The sloping lines have an associated equation that may be used directly, with the appropriate GBA value. We have included the figures, instead of equations only, to illustrate the dramatic reduction in the coefficients with increasing GBA values.

In each figure, only GBA values in the range of 0 to 0.3 are presented corresponding to available data. The following special conditions hold:

(a) GBA = 0.01 for row 1 with no external fence, and

(b) GBA = 0.02 for row 2 with no external fence.

Note that load coefficients for these first two rows without external fence may be larger in magnitude than the coefficients for an isolated unit.

It should be noted that data for this guideline were obtained in array fields with a regular pattern as shown in Figure 24. Data were not obtained for other array geometries.

LOAD COMBINATION COEFFICIENTS WITHIN A FIELD

Load combinations within a field of heliostats or parabolic dishes at conditions other than those where one component is a maximum are presented in this

Heliostats

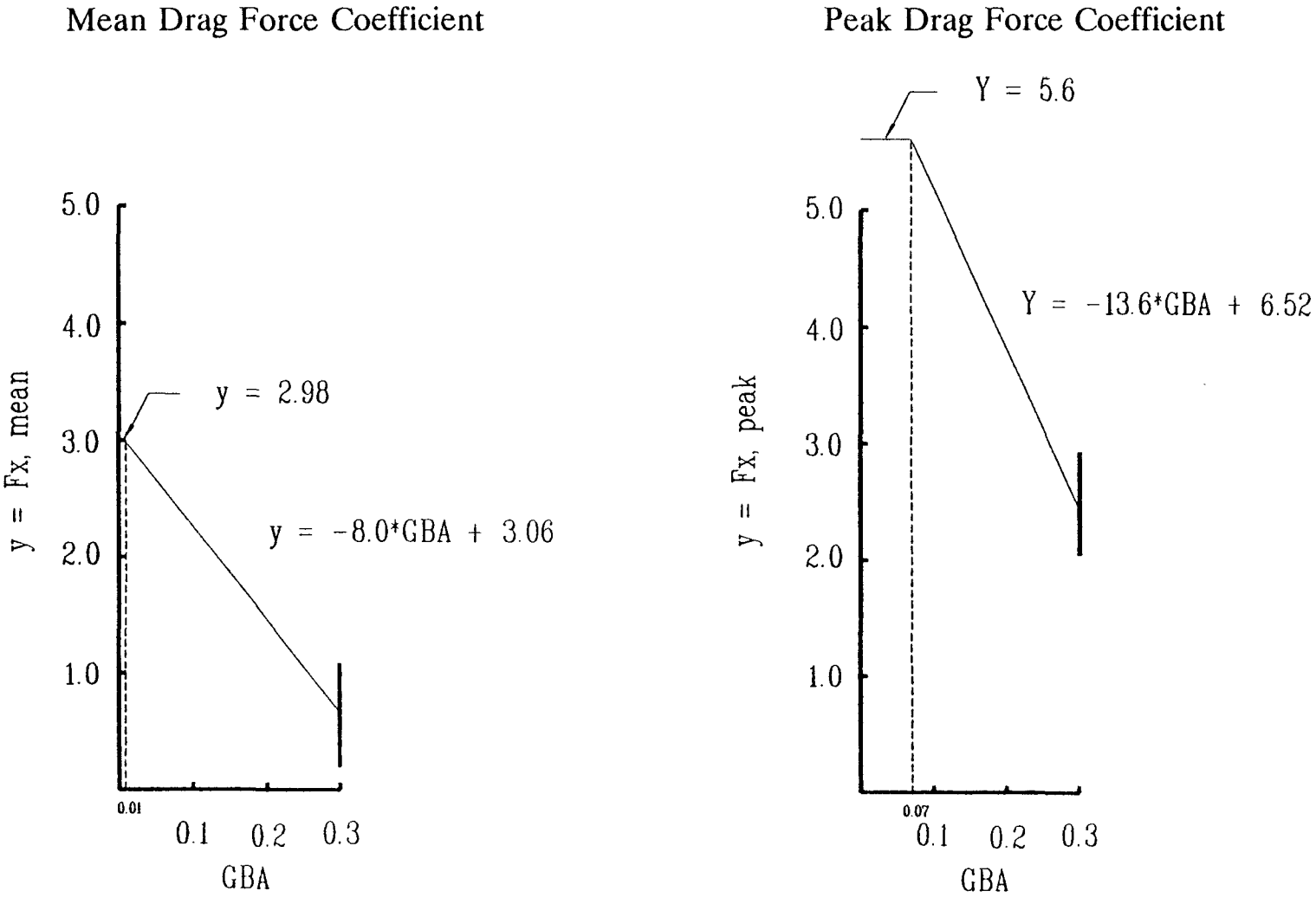

Figure 25. Mean and peak drag force coefficients, Fx, of a heliostat unit within a field of heliostats.

Heliostats

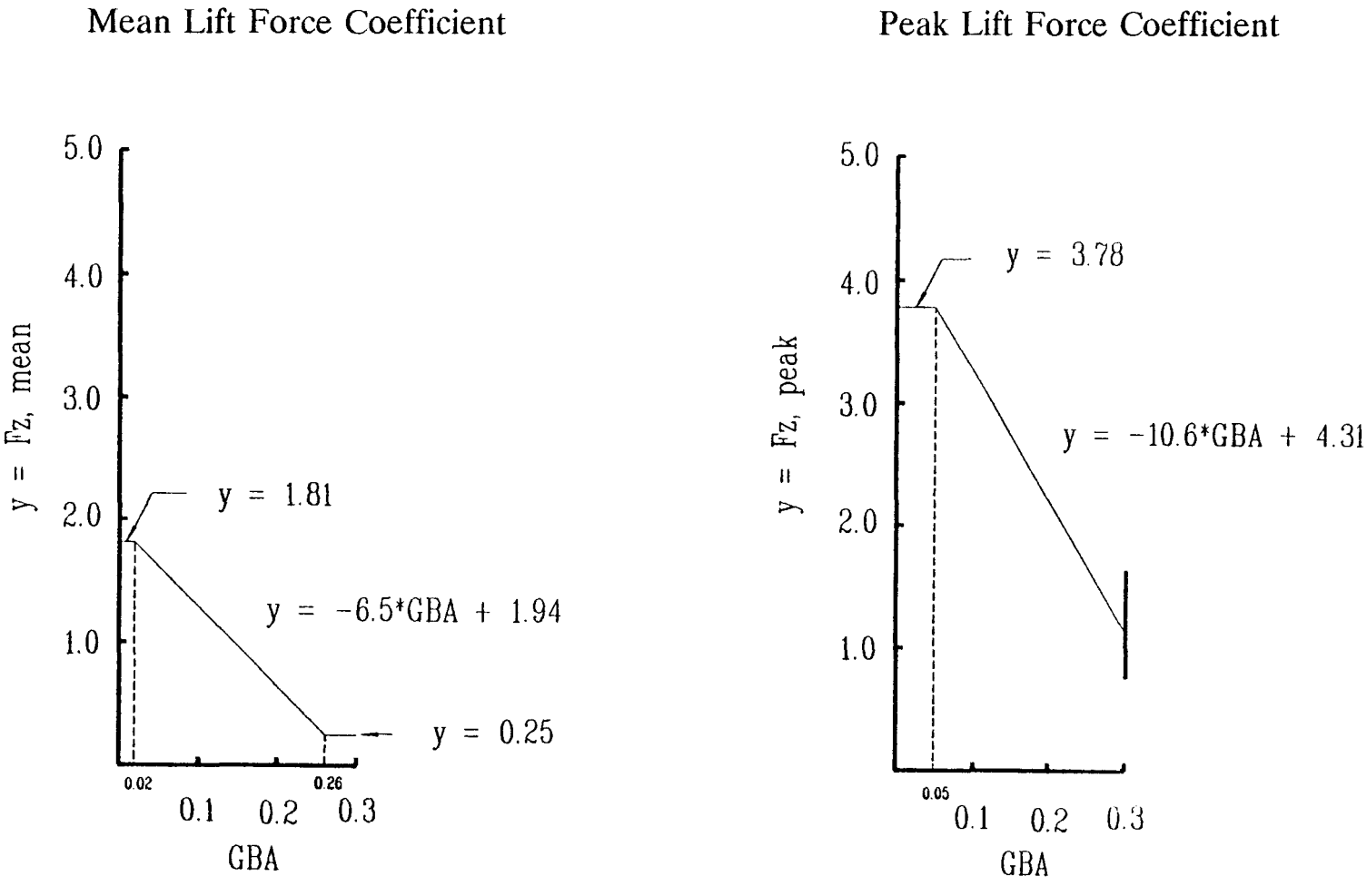

Figure 26. Mean and peak lift force coefficients, Fz, of a heliostat unit within a field of heliostats.

Heliostats

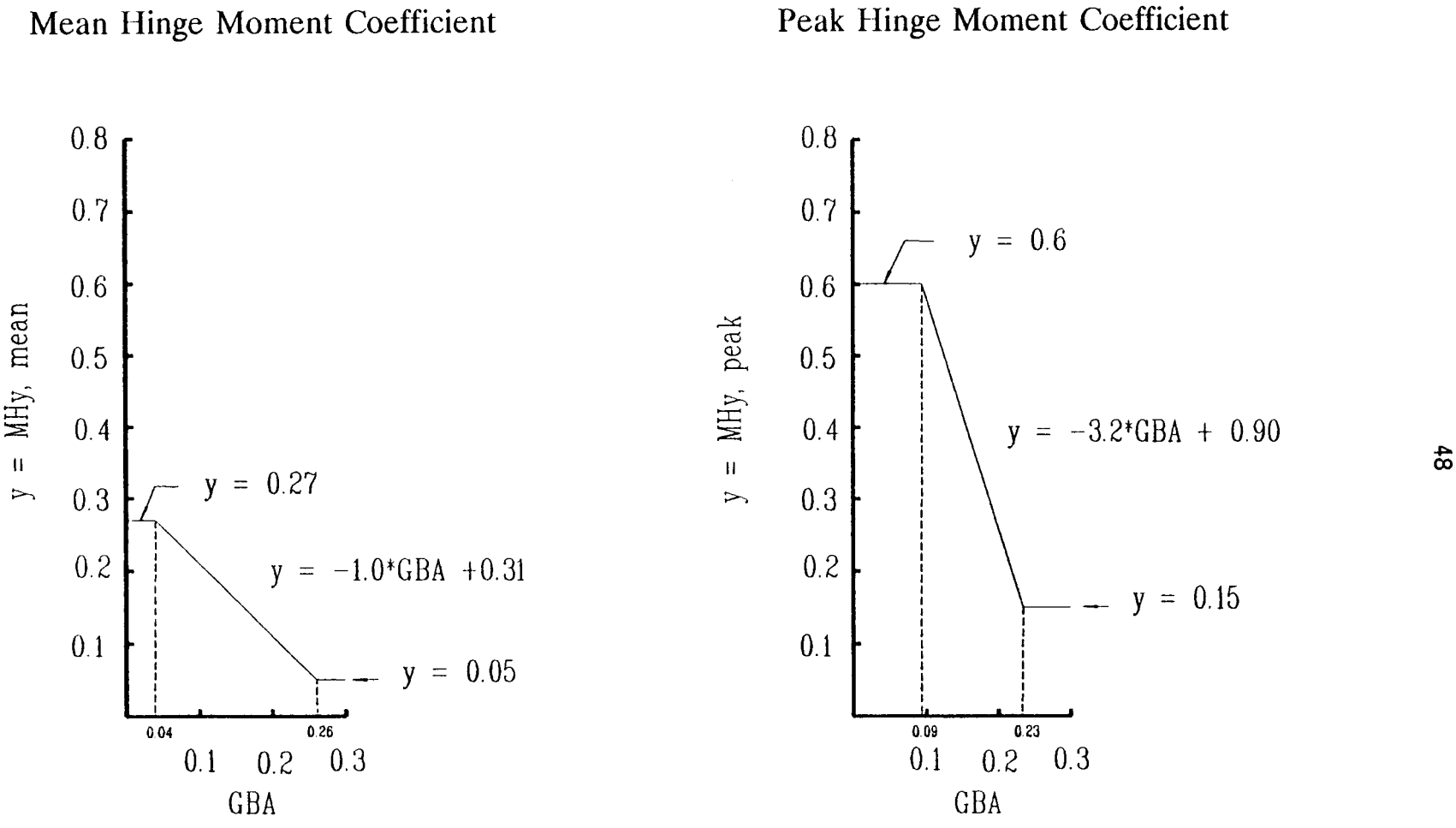

Figure 27. Mean and peak hinge moment coefficients, MHy, of a heliostat unit within a field of heliostats.

Heliostats

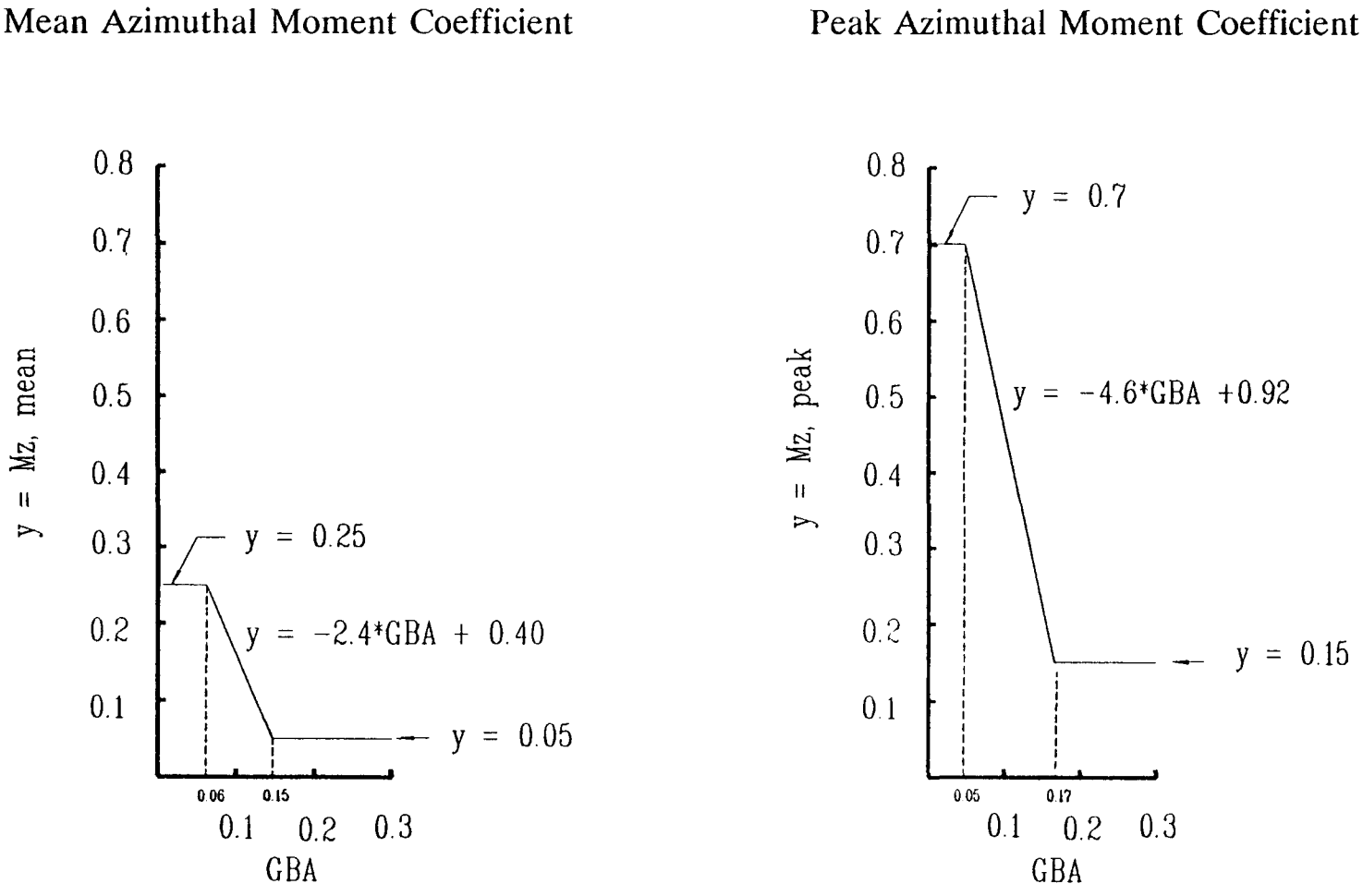

Figure 28. Mean and peak azimuthal moment coefficients, Mz, of a heliostat unit within a field of heliostats.

Parabolic Dishes

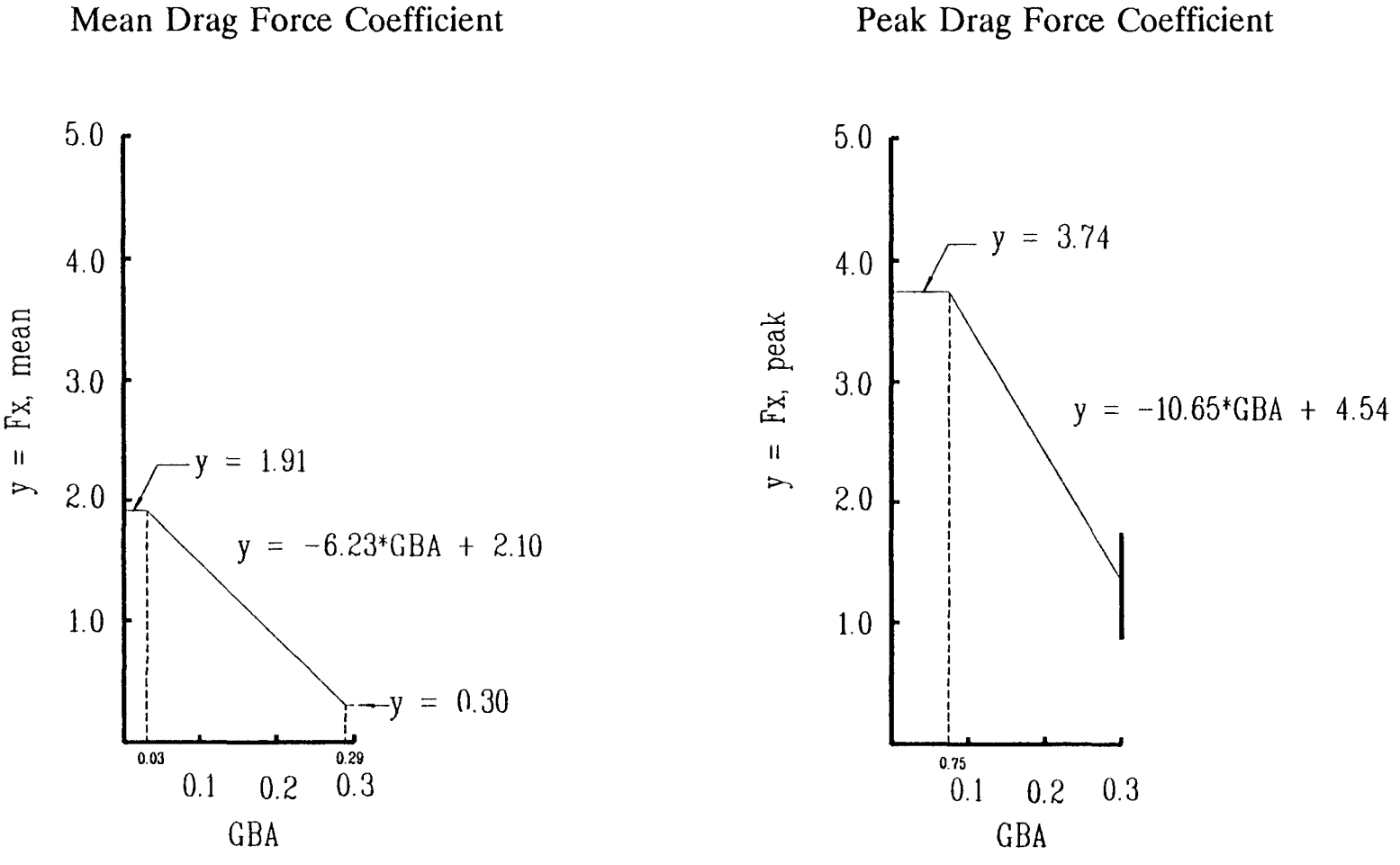

Figure 29. Mean and peak drag force coefficients, Fx, of a parabolic dish unit within a field of parabolic dishes.

Parabolic Dishes

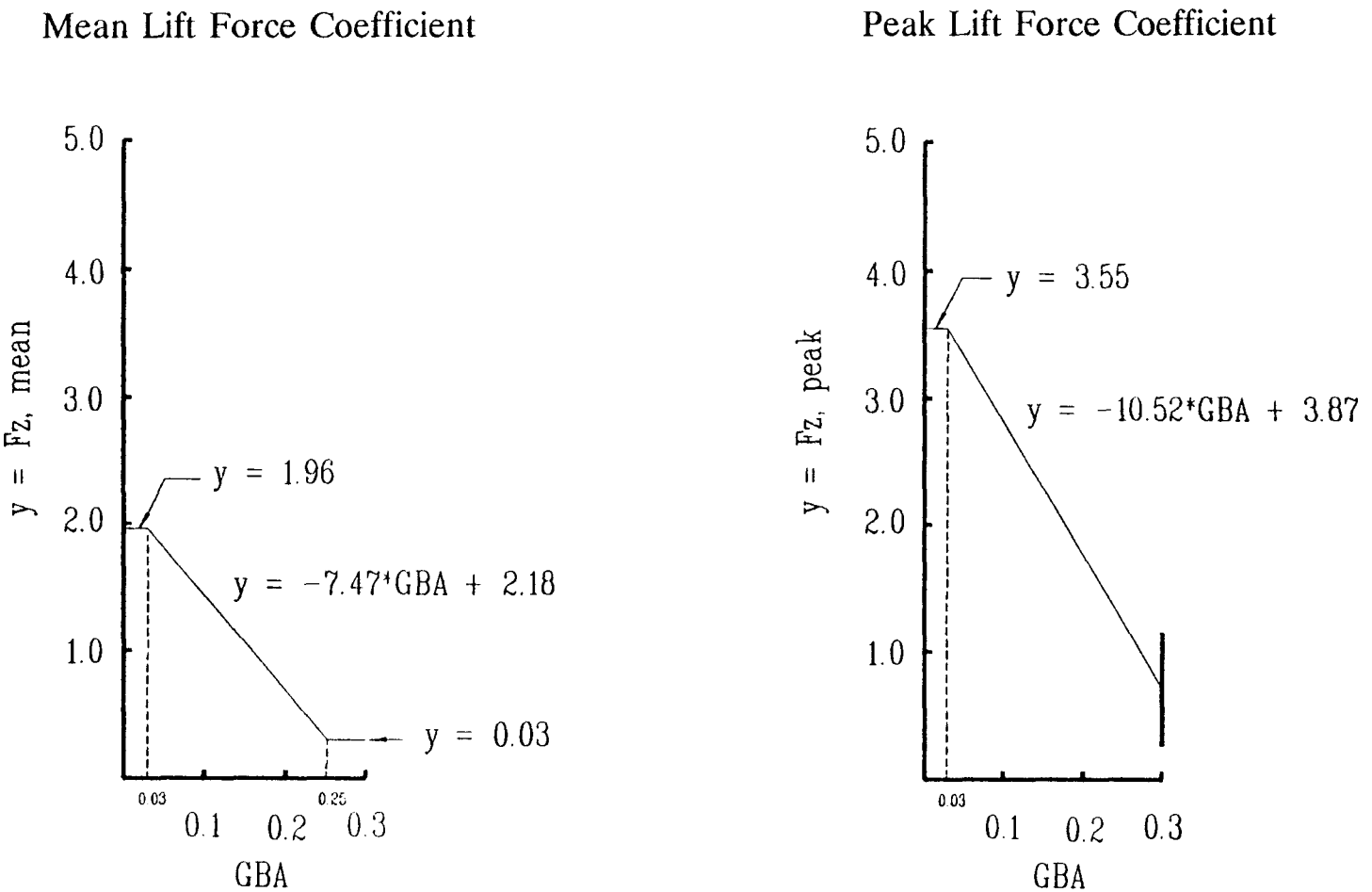

Figure 30. Mean and peak lift force coefficients, Fz, of a parabolic dish unit within a field of parabolic dishes.

Parabolic Dishes

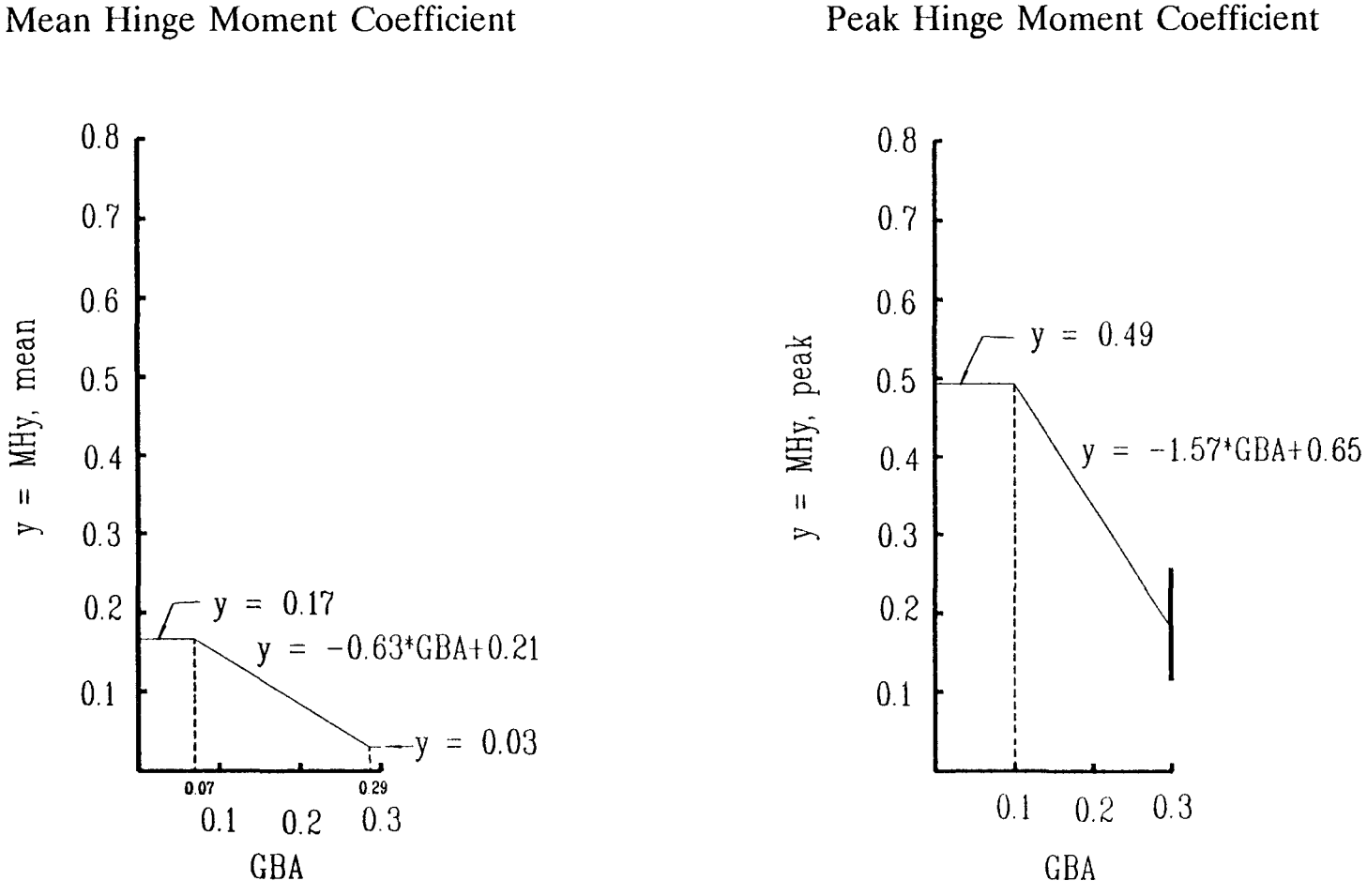

Figure 31. Mean and peak hinge moment coefficients, MHy, of a parabolic dish unit within a field of parabolic dishes.

Parabolic Dishes

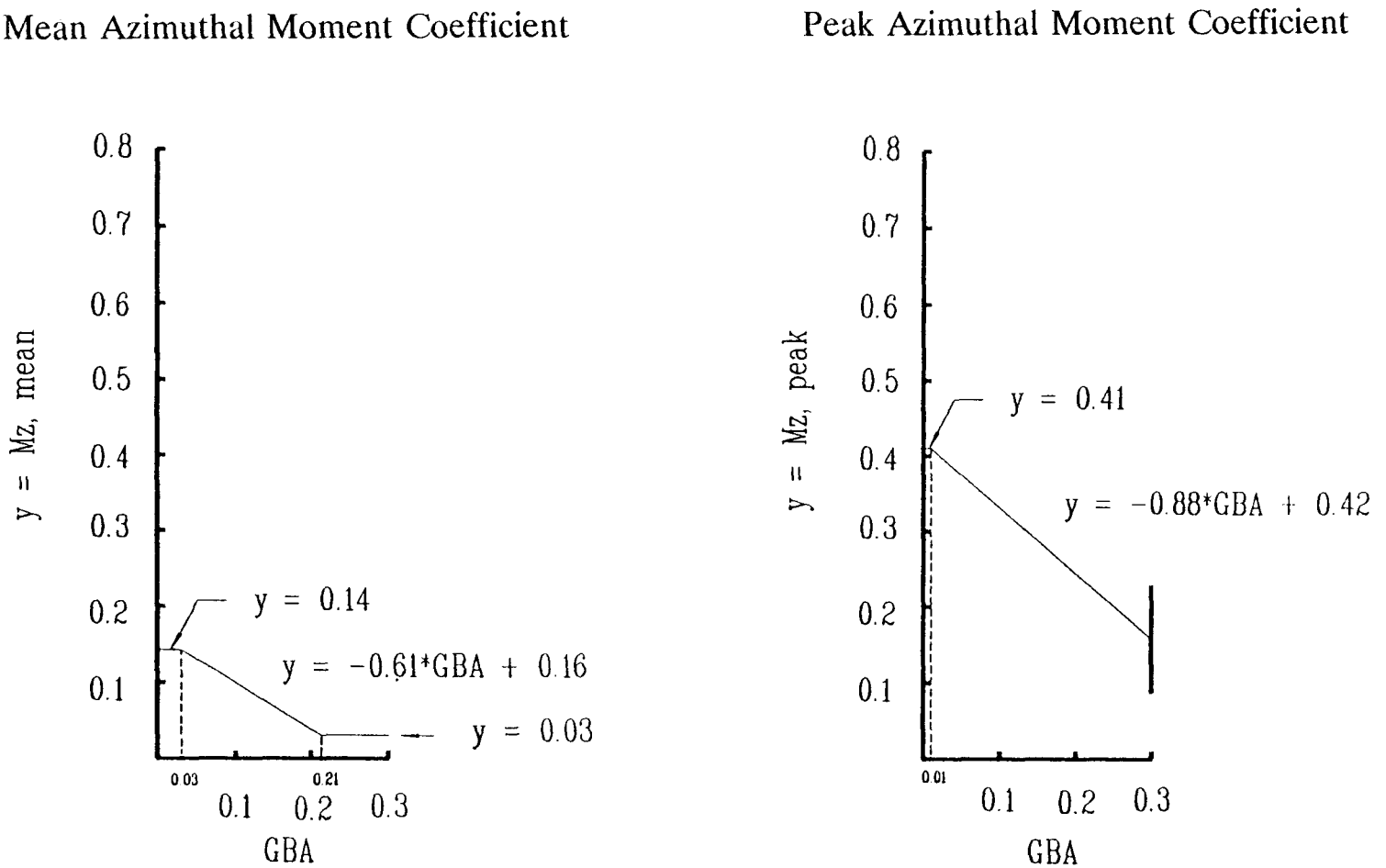

Figure 32. Mean and peak azimuthal moment coefficients, Mz, of a parabolic dish unit within a field of parabolic dishes.

section. Because the research leading to this method was directed at obtaining maximum loads, there is very little data to support the calculation of load combinations in a field. What data exists tends to show smaller reductions within a field than occurs for the largest values of component loads. For that reason, what data was available is presented. While the data presented here is thought to be reasonable and conservative for design use, there is no guarantee that the data used to prepare this section found the largest load combination values. The data are presented with the caveat that use of this data might lead to under-prediction of some loads. The data leading to the results of this section were obtained for GBA values near 0.1.

Tables 4 and 5 show factors to be used as multipliers of coefficients shown in Figures 4 to 15. The data are divided into four classifications: heliostats or parabolic dish collectors with and without an external wind fence with porosity no larger than 30 to 50 percent.

Table 4. Multiplying factors for isolated load combinations for in-field heliostat performance.

(a) without external fence

Row	1	2	3	4
$F_{x,peak}$	0.69	0.69	0.69	0.69
$F_{x,mean}$	1.01	0.76	0.73	0.69
$F_{z,peak}$	0.93	0.95	0.91	0.72
$F_{z,mean}$	1.26	1.15	1.03	0.86
$M_{Hy,peak}$*	-	-	-	-
$M_{Hy,mean}$*	-	-	-	-
$M_{z,peak}$	0.51	0.66	0.70	0.72
$M_{z,mean}$	0.68	0.78	0.96	0.95

(b) with external fence

Row	1	2	3	4
$F_{x,peak}$	0.25	0.56	0.65	0.69
$F_{x,mean}$	0.26	0.48	0.56	0.69
$F_{z,peak}$	0.32	0.48	0.57	0.72
$F_{z,mean}$	0.32	0.53	0.72	0.86
$M_{Hy,peak}$*	-	-	-	-
$M_{Hy,mean}$*	-	-	-	-
$M_{z,peak}$	0.25	0.54	0.72	0.72
$M_{z,mean}$	0.43	0.62	0.98	0.95

* insufficient data

Note: For cases where a component load is near its maximum, use Figures 25 to 28 instead of this table.

Table 5. Multiplying factors for isolated load combinations for in-field parabolic dish performance.

(a) without external fence

Row	1	2	3	4
$F_{x,peak}$	1.07	1.00	0.97	0.93
$F_{x,mean}$	1.03	0.81	0.58	0.55
$F_{z,peak}$	1.10	1.04	0.88	0.80
$F_{z,mean}$	1.06	0.76	0.63	0.61
$M_{Hy,peak}$	1.07	1.07	1.06	1.16
$M_{Hy,mean}$	1.07	0.78	0.75	0.72
$M_{z,peak}$	1.00	1.38	1.26	1.27
$M_{z,mean}$	0.94	0.94	0.94	0.94

(b) with external fence

Row	1	2	3	4
$F_{x,peak}$	0.45	0.71	0.86	0.93
$F_{x,mean}$	0.36	0.43	0.54	0.55
$F_{z,peak}$	0.48	0.70	0.75	0.80
$F_{z,mean}$	0.44	0.52	0.65	0.61
$M_{Hy,peak}$	0.60	0.92	1.04	1.16
$M_{Hy,mean}$	0.37	0.55	0.65	0.72
$M_{z,peak}$	0.46	0.90	1.12	1.27
$M_{z,mean}$	0.43	0.61	0.96	0.94

Note: For cases where a component load is near its maximum, use Figures 29 to 32 instead of this table.

EXAMPLE PROBLEM 1

An example problem is presented for an in-field heliostat to demonstrate the calculation of peak wind forces and moments when a collector is embedded within an array. The same procedure is followed for an in-field parabolic dish. For an isolated heliostat or parabolic dish, Step 1 and Step 3 are omitted and Table 2 or Table 3 are used directly in Step 4.

PROBLEM: Calculate peak operational drag force, lift force, hinge moment, and azimuthal moment for a 40 x 40 foot square heliostat with a center, H, 22 ft above ground. Perform calculation for (a) heliostat in third row and (b) heliostat in fifth row.

Given: H = 22 ft; a 25 ft-high external fence with a 50% porosity is located 80 ft from edge of field of collectors; no internal fences; heliostat spacing is 80 ft along rows (parallel to external fence) and 80 ft between rows (perpendicular to fence). Wind has peak gust speed of 55 mph at 10 m (32.8 ft) elevation.

Note: Refer to Figures 1 and 24 in doing this problem. Coefficient values for an in-field heliostat are presented in Figures 25 through 28. If the calculations were to be performed for an isolated heliostat, use Table 2 in place of Figures 25 to 28.

Step 1. GBA Calculations (see Figure 4 and Eqs. (1) through (6)).

(a) Heliostat at the third row

$AF = (160 + 80) \times 80 = 19200\ ft^2$ (includes 2 upwind collectors and external fence)

$AS = 80 \times 25 \times 50\% = 1000\ ft^2$ (external wind fence only)

$AH = 2 \times 40 \times 40 = 3200\ ft^2$ (2 upwind collectors included as shown in Figure 24)

$$\text{For Fx: } GBA = \frac{K \quad AH \quad AS}{AF} \quad GBA$$

$$GBA = \frac{1.0 \times 3200 + 1000}{19200} = 0.219$$

$$\text{Fz: } GBA = \frac{0.5 \times 3200 + 1000}{19200} = 0.135$$

$$\text{MHy: } GBA = \frac{0.5 \times 3200 + 1000}{19200} = 0.135$$

$$\text{Mz: } GBA = \frac{0.5 \times 3200 + 1000}{19200} = 0.135$$

(b) Heliostat at the fifth row

$AF = 160 \times 80 = 12800\ ft^2$ (2 upwind collectors included as shown in Figure 24)

$AS = 0.0\ ft^2$ (external fence is not effective at 5th row)

$AH = 2 \times 40 \times 40 = 3200\ ft^2$

$$\text{For Fx: } GBA = \frac{K \quad AH \quad AS}{AF} \quad GBA$$

$$GBA = \frac{1.0 \times 3200 + 0.0}{12800} = 0.25$$

$$Fz: \quad GBA = \frac{0.5 \times 3200 + 0.0}{12800} = 0.125$$

$$MHy: \quad GBA = \frac{0.5 \times 3200 + 0.0}{12800} = 0.125$$

$$Mz: \quad GBA = \frac{0.5 \times 3200 + 0.0}{12800} = 0.125$$

Step 2. Dynamic pressure calculation

U_{mean} at 10 m = $U_{gust}/1.6$ = 55/1.6 = 34.4 mph

H = 22 ft, Z_{wind} = 10 m = 32.8 ft

Open country terrain, n = 0.14

$$U_{mean} \text{ at } H = 34.4 \left(\frac{22}{32.8}\right)^{0.14} = 32.5 \text{ mph}$$

$$Q = 0.00256 \times 32.5^2 = 2.70 \text{ lb/ft}^2$$

Step 3. Maximum coefficients on the bounding curves (use Figures 25 through 28 for heliostats)

(a) The third row

		Slope	GBA	Const.	
Peak:	CFx = (	-13.6 x	0.219 +	6.52)	= 3.54

CFz = (-10.6 x 0.135 + 4.31) = 2.88

CMHy = (-3.2 x 0.135 + 0.90) = 0.468

CMz = (-4.6 x 0.135 + 0.92) = 0.299

(b) The fifth row

Peak: $CFx = (-13.6 \times 0.25 + 6.52) = 3.12$

$CFz = (-10.6 \times 0.125 + 4.31) = 2.98$

$CMHy = (-3.2 \times 0.125 + 0.90) = 0.50$

$CMz = (-4.6 \times 0.125 + 0.92) = 0.345$

The calculation of the base overturning moment, CMy for the third and fifth rows is determined from Eq. (6):

$CM_{base} = CMy = CFx + CMHy \times (h/H)$ (h = 40 ft in this problem)

Step 4. Forces and moments (refer to Eqs. (1) through (6))

(a) The third row

Peak: $Fx = 3.54 \times 2.70 \times 1600 = 15300$ lb

$Fz = 2.88 \times 2.70 \times 1600 = 12400$ lb

$M_{base} = My = (3.54 + 0.468 \times 40/22) \times 2.70 \times 1600 \times 22$
$= 4.18 \times 10^5$ lb-ft

$M_{hinge} = MHy = 0.468 \times 2.70 \times 1600 \times 40$
$= 8.14 \times 10^4$ lb-ft

$M_{azimuth} = Mz = 0.329 \times 2.70 \times 1600 \times 40$
$= 5.54 \times 10^4$ lb-ft

(b) The fifth row

Peak: $Fx = 3.12 \times 2.70 \times 1600 = 13500$ lb

$Fz = 2.98 \times 2.70 \times 1600 = 12900$ lb

$M_{base} = My = (3.12 + 0.50 \times 40/22) \times 2.70 \times 1600 \times 22$

$= 3.83 \times 10^5$ lb-ft

$M_{hinge} = MHy = 0.50 \times 2.70 \times 1600 \times 40$

$= 8.72 \times 10^4$ lb-ft

$M_{azimuth} = Mz = 0.375 \times 2.70 \times 1600 \times 40$

$= 6.36 \times 10^4$ lb-ft

EXAMPLE PROBLEM 2

An example problem is presented for an isolated or in-field parabolic dish to demonstrate the calculation of peak load combinations for the major components of the collector where loads are not at their largest values. The same procedure is followed for a heliostat.

Problem: Calculate the peak load combination of the major structural components for a parabolic dish with a diameter, h, of 40 feet. The dish is in the second row of an array of collectors. Perform the calculations with and without an external fence.

Givens: 1) H = 22 ft (height of center of dish from ground), 2) wind has a peak gust speed of 55 mph at 10 m (32.8 ft) elevation, 3) wind direction, β, is 50°, 4) collector tilt, α, is 70°, and 5) open country terrain.

Note: Refer to Figure 1, to Figures 8 to 15, and to Table 5 in solving this problem.

Step 1. Dynamic pressure calculation. See Example Problem 1.

$Q = 0.00256\ (32.5)^2 = 2.70\ lb/ft^2$.

Step 2. Calculate isolated collector peak loads for $\beta = 50°$ and $\alpha = 70°$.

(a) Drag force, F_x (Figure 9 and Eq. (1))

$$F_{x,peak} = \underset{C_{Fx}}{(3.0)}\ \underset{Q}{(2.70)}\ \underset{A}{(1257)} = 10{,}200\ lb$$

where $A = \pi h^2/4$ is collector area.

(b) Lift force, F_z (Figure 11 and Eq. (2))

$$F_{z,peak} = \underset{C_{Fz}}{(-0.95)}\ \underset{Q}{(2.70)}\ \underset{A}{(1257)} = -3200\ lb$$

(c) Azimuthal moment, M_z (Figure 13 and Eq. (5))

$$M_{z,peak} = \underset{C_{Mz}}{(0.30)}\ \underset{Q}{(2.70)}\ \underset{A}{(1257)}\ \underset{h}{(40)} = 40{,}700\ lb\text{-}ft$$

(d) Hinge moment, MH_y (Figure 15 and Eq. (4))

$$MH_{y,peak} = \underset{CMH_y}{(0.28)}\ \underset{Q}{(2.70)}\ \underset{A}{(1257)}\ \underset{h}{(40)} = 38{,}000 \text{ lb-ft}$$

(e) Base overturning moment, My (Eqs. (3) and (6))

$$C_{My,peak} = \underset{CF_x}{3.0} + \underset{CMH_y}{0.28}\ \underset{h,H}{\left[\frac{40}{22}\right]} = 3.51$$

Therefore, the peak base overturning moment is

$$M_{y,peak} = \underset{CM_y}{(3.51)}\ \underset{Q}{(2.70)}\ \underset{A}{(1257)}\ \underset{H}{(22)} = 2.62 \times 10^5 \text{ lb-ft}$$

Step 3. Calculate in-field collector performance at second row for $\beta = 50°$ and $\alpha = 70°$. See text for discussion of Table 5.

(a) Drag force, F_x (use values from Step 2 and Table 5)

Without external fence:

$$F_{x,peak} = \underset{\text{isolated}}{(10{,}200)}\ \underset{\text{Tbl 5}}{(1.00)} = 10{,}200 \text{ lb}$$

With external fence:

$$F_{x,peak} = (10{,}200)\ (0.71) = 7000 \text{ lb}$$

(b) Lift force, F_z

Without external fence:

$F_{z,peak}$ = (-3200) (1.04) = -3300 lb

With external fence:

$F_{z,peak}$ = (-3200) (0.70) = -2200 lb

(c) Azimuthal moment, M_z

Without external fence:

$M_{z,peak}$ = (40,700) (1.38) = 56,200 lb-ft

With external fence:

$M_{z,peak}$ = (40,700) (0.90) = 36,600 lb-ft

(d) Hinge moment, MH_y

Without external fence:

$MH_{y,peak}$ = (38,000) (1.07) = 40,700 lb-ft

With external fence:

$MH_{y,peak}$ = (38,000) (0.90) = 34,200 lb-ft

From this example problem one can see the obvious advantages of an external wind fence in reducing loads for an in-field collector in the second row. The above calculations yield a component load combination for one specific collector orientation and in-field placement wind direction, and wind speed. The method

allows for a wide range of collector orientations and placements in studying load combinations.

REFERENCES

ANSI/ASCE 7-88, (1988), "Minimum Design Loads For Buildings and Other Structures," American Society of Civil Engineers and American National Standards Association, 1988 version of the national wind load standard.

ASCE, (1961), "Wind Forces On Structures," Transactions of the American Society of Civil Engineers, Paper 3269, Vol. 126, p. 1124.

Cermak, J. E., (1975), "Applications of Fluid Mechanics to Wind Engineering," A Freeman Scholar Lecture, ASME, Jl. of Fluid Engineering, Vol. 97, No. 1.

Cermak, J. E., (1971), "Laboratory Simulation of the Atmospheric Boundary Layer," AIAA Jl., Vol. 9.

Counihan, J., (1975), "Adiabatic Atmospheric Boundary Layers: A Review and Analysis of Data from the Period 1880-1972," Atmospheric Environment, Vol. 9, pp. 871-905.

ESDU, (1982), "Strong Winds in the Atmospheric Boundary Layer: Part 1: Mean-hourly Wind Speeds," Item No. 82026, ESDU International Ltd., London.

Hollister, S. C., (1970), "The Engineering Interpretation of Weather Bureau Records for Wind Loading on Structures," Building Science Series 30 -- Wind Loads on Buildings and Structures, National Bureau of Standards, pp. 151-164.

Peglow, S. G., (1979), "Wind-Tunnel Study of a Full-Scale Heliostat," Sandia Laboratories Report, DOE Contract DE-AC04-760P00789.

Peterka, J. A., R. G. Derickson and J. E. Cermak, (1990), "Wind Loads and Local Pressure Distributions on Parabolic Dish Collectors," Solar Energy Research Institute Report SERI/TP-253-3668, Golden, CO.

Peterka, J. A., Z. Tan, J. E. Cermak and B. Bienkiewicz, (1989) "Mean and Peak Wind Loads on Heliostats," Transactions of the ASME, Jl. of Solar Energy Engineering, Vol. 111, May, pp. 158-164.

Peterka, J. A., Z. Tan, B. Bienkiewicz and J. E. Cermak, (1988), "Wind Loads on Heliostats and Parabolic Dish Collectors," SERI/STR-253-3431, Technical Report for Solar Energy Research Institute, Golden, CO.

Peterka, J. A., Z. Tan, B. Bienkiewicz and J. E. Cermak, (1987), "Mean and Peak Wind Load Reduction on Heliostats," SERI/STR-253-3212, DE87012281, Solar Energy Research Institute, Golden, CO.

Peterka, J. A., N. Hosoya, B. Bienkiewicz and J. E. Cermak, (1986), "Wind Load Reduction For Heliostats," Solar Energy Research Institute Report SERI/STR-253-2859, Golden, CO.

Reinhold, T. A. (Ed.) (1982), Wind Tunnel Modeling for Civil Engineering Applications, Proceedings of an International Workshop, Cambridge University Press, NY.

Simiu, E. and R. H. Scanlan, (1986), Wind Effects on Structures, 2nd Edition, John Wiley & Sons.

UNLIMITED DISTRIBUTION
INITIAL DISTRIBUTION
REVISION 12/2/91/jwg

U.S. Department of Energy (4)
Forrestal Building Code
CE-132 1000
Independence Avenue, SW
Washington, DC 20585
Attn: G. Burch
S. Gronich

U.S. Department of Energy (2)
Forrestal Building
Code CE-13
1000 Independence Avenue, SW
Washington, DC 20585
Attn: B. Annan

U.S. Department of Energy
Forrestal Building Code
CE-10
1000 Independence Avenue, SW
Washington, DC 20585
Attn: R. San Martin

U.S. Department of Energy (3)
Albuquerque Operations Office
P.O. Box 5400
Albuquerque,NM 87115
Attn: C. Garcia
G. Tennyson
N. Lackey

U.S. Department of Energy
San Francisco Operations Office
1333 Broadway
Oakland, CA 94612
Attn: R. Hughey

Acurex Corporation (2)
555 Clyde Avenue
Mountain View, CA 94039
Attn: H. Dehne

Advanced Thermal Systems
7600 East Arapahoe
Suite 319 Englewood, CO 80112
Attn: D. Gorman

Allegheny Ludlum Steel
80 Valley Street
Wallingford, CT 06492
Attn: J. Halpin

Analysis Review & Critique
6503 81st Street
Cabin John, MD 20818
Attn: C. LaPorta

Arizona Public Service Company
P.O. Box 53999
M/S 9110
Phoenix,AZ 85072-3999
Attn: W. J. McGuirk

Arizona Solar Energy Office
3800 North Central
Phoenix, AZ 85012
Attn: R. Williamson

Australian National University
Department of Engineering Physics
P. O. Box 4
Canberra ACT 2600 AUSTRALIA
Attn: S. Kaneff

Barber-Nichols Engineering
6325 West 55th Avenue
Arvada, CO 80002
Attn: R. Barber

Battelle Pacific Northwest Laboratory (2)
P.O. Box 999
Richland,WA 99352
Attn: D. Brown

BDM Coporation
1801 Randolph Street
Albuquerque,NM 87106
Attn: W. Schwinkendorf

Bechtel National, Inc.
50 Beale Street
50/15 D8
P. O. Box 3965
San Francisco, CA 94106
Attn: P. DeLaquil

Black & Veatch ConsultingEngineers
P.O. Box 8405
Kansas City, MO 64114
Attn: J. C. Grosskreutz

Tom Brumleve
1512 Northgate Road
Walnut Creek, CA 94598

California Energy Commission
1516 Ninth Street, M-S 43
Sacramento, CA 95814
Attn: A. Jenkins

California Polytechnic University
Dept. of Mechanical Engineering
Pomona, CA 91768
Attn: W. Stine

California Public Utilities Com.
Resource Branch, Room 5198
455 Golden Gate Avenue
San Francisco, CA 94102
Attn: T. Thompson

Cummins Engine Co.
MC 60125
P. O. Box 3005
Columbus, IN 47202-3005
Attn: R. Kubo

Cummins Power Generation,Inc.,South
150 Tanne Hill Drive
Abilene, Texas 79602
Attn: M. McGlaun

Dan Ka
3905 South Mariposa
Englewood, CO 80110
Attn: D. Sallis

DLR
Pfaffenwaldring 38-40
7000 Stuttgart 80
FEDERAL REPUBLIC OF GERMANY
Attn: R. Buck

DLR (2)
Linder Hohe
5000 Koln 90
FEDERAL REPUBLIC OF GERMANY
Attn: M. Becker
M. Bohmer

DSET
P. O. Box 1850
Black Canyon Stage I
Phoenix, AZ 85029
Attn: G. Zerlaut

Electric Power Research Institute
P.O. Box 10412
Palo Alto, CA 94303
Attn: J. Schaeffer

Engineering Perspectives
20 19th Avenue
San Francisco, CA 94121
Attn: John Doyle

Energy Technology Engr. Center
Rockwell International Corp.
P. O. Box 1449
Canoga Park, CA 91304
Attn: W. Bigelow

ENIECH, Inc.
P. O. Box 612246
DFW Airport,TX 75261
Attn: R. Walters

Flachglas Solartechnik GmbH
Muhlengasse7
D-5000 Koln 1
FEDERAL REPUBLIC OF GERMANY
Attn: J. Benemann

Flachglas Solartechnik GmbH
Sonnefistr. 25
D-8000 Munchen 1
FEDERAL REPUBLIC OF GERMANY
Attn: M. Geyer

Florida Solar Energy Center
300 State Road 401
Cape Canaveral, FL 32920
Attn: Library

Ford Aerospace
Ford Road
Newport Beach, CA 92663
Attn: R. Babbe

Foster Wheeler Solar Development
Corporation (2)
12 Peach Tree Hill Road
Livingston, NJ 07039
Attn: M. Garber
R. Zoschak

Garrett Turbine Engine Co.
111 South 34th Street
P. O. Box 5217
Phoenix, AZ 85010
Attn: E. Strain

Georgia Power (2)
7 Solar Circle
Shenandoah, GA 30265
Attn: W. King

Harris Corporation (2)
Govermnent and Aerospace Systems
Division
P. O. Box 9400
Melbourne, FL 32902
Attn: K. Schumacher

Industrial Solar Technologies
5775 West 52nd Avenue
Denver, CO 80212
Attn: R. Gee

Institute of Gas Technology
34245 State Street
Chicago, IL 60616
Attn: Library

ISEIR
951 Pershing Drive
Silver Spring,MD 20910
Attn: A. Frank

Lawrence Berkeley Laboratory
MS 90-2024
One Cyclotron Road
Berkeley, CA 94720
Attn: A. Hunt

Luz International (2)
924 Westwood Blvd.
Los Angeles, CA 90024
Attn: D. Kearney

3M-Energy Control Products (2)
207-lW 3M Center
St. Paul, MN 55144
Attn: R. Dahlen

Mechanical Technology, Inc. (2)
968 Albany Shaker Road
Latham,NY 12110
Attn: G. Dochat
J. Wagner

Meridian Corporation
4300 King Street
Alexandria,VA 22302
Attn: D. Kumar

NASA Lewis Research Center (4)
21000 Brook Park Road
Cleveland, OH 44135
Attn: R. Corrigan,500-221
L. Greenlee, 500-221
T. Mroz, 301-5
J. Calogeras, 301-5

Nevada Power Co.
P. O. Box 230
Las Vegas, NV 89151
Attn: Mark Shank

NREL (5)
1617 Cole Boulevard
Golden, CO 80401
Attn: T. Williams
L.M. Murphy
G. Jorgensen
T. Wendelin
A. Lewandowski

Pacific Gas and Electric Company (2)
3400 Crow Canyon Road
San Ramon, CA 94526
Attn: G. Braun
J. Iannucci

Peerless Winsmith, Inc.
172 Eaton Street
P. O. Box 530 Springville, NY 14141
Attn: W. Heller

Polydyne, Inc.
1900 S. Norfolk Street, Suite 209
San Mateo, CA 94403
Attn: P. Bos

Power Kinetics, Inc.
415 River Street
Troy,NY 12180-2822
Attn: W. Rogers

Rocketdyne Division
6633 Canoga Park Ave.
Canoga Park,CA 91304
Attn: W. Marlatt

San Diego Gas and Electric Company
P.O. Box 1831
San Diego,CA 92112
Attn: R. Figueroa

SCE
P. O. Box 800
Rosemead, CA 91770
Attn: C. Lopez

Schlaich, Bergennann & Partner
Hohenzollernstr. 1
D - 7000 Stuttgart 1
West Germany
Attn: W. Schiel

Science Applications International Corporation (2)
10343 Roselle Street, Suite G
San Diego, CA 92121
Attn: K. Beninga
J. Sandubrae

Science Applications International Corporation
Mail Stop 32
10206 Campus Point Court
San Diego, CA 92121
Attn: B. Butler

Solar Kinetics, Inc. (2)
P.O. Box 540636
Dallas, TX 75354-0636
Attn: J. A. Hutchison
P. Schertz
D. Konnerth

Solar Power Engineering Company
P.O. Box 91
Morrison, CO 80465
Attn: H. Wroton

Solar Steam
P. O. Box 32
Fox Island, WA 98333
Attn: D. Wood

SRS Technologies
990 Explorer Blvd., NW
Huntsville, AL 35806
Attn: R. Bradford

Stearns Catalytic Corporation
P.O. Box 5888
Denver, CO 80217
Attn: T. E. Olson

Stirling Thermal Motors
275 Metty Drive
AnnArbor, MI 48103
Attn: T. Godett

Sun Power, Inc.
6 Byard Street
Athens, OH 45701
Attn: W. Beale

Tom Tracey
6922 South Adams Way
Littleton, CO 80122

United Solar Tech, Inc.
3434 Martin Way
Olympia, WA 98506
Attn: R. Kelley

University of Chicago
Enrico Fermi Institute
5640 Ellis Avenue
Chicago, IL 60637
Attn: J. O'Gallagher

University of Houston
Solar Energy Laboratory
4800 Calhoun
Houston, TX 77704
Attn: L. Vant-Hull

University of Utah
Mechanical and Industrial Engineering
Salt Lake City, UT 84112
Attn: B. Boehm

Eric Weber
302 Caribbean Lane
Phoenix, AZ 85022

WGAssociates
6607 Stonebrook Circle
Dallas, TX 75240
Attn: V. Goldberg

140 R. E. Loehman
1846 D. H. Doughty
1846 C. S. Ashley
7141 Technical Library (5)
7613-2 Document Processing (10)
for DOE/OSTI
7151 Technical Publications
4051 Disclosure Division (3)
6000 D. L. Hartley
6200 B. W. Marshall
6215 C. P. Cameron
6215 R. M. Houser
6216 C. E. Tyner
6216 L. Yellowhorse
6216 D. J. Alpert
6216 J. W. Grossman (20)
6216 T. R. Mancini (3)
6216 J. E. Pacheco
6217 P. C. Klimas
6217 R. B. Diver
6220 D. G. Schueler
6221 T. C. Bickel
6221 A. R. Mahoney
6223 G. J. Jones
6224 D. E. Hasti
7470 J. L. Ledman
7476 F. P. Gerstle
7476 S. T. Reed
8523-2 Central Technical Files